Whither second-sphere coordination?

Liu, W., Das, P. J., Colquhoun, H. M. and Stoddart, J. F. (2022) Whither second-sphere coordination? CCS Chemistry, 4 (3). pp. 755-784. ISSN 2096-5745 doi: https://doi.org/10.31635/ccschem.021.202101286 Available at https://centaur.reading.ac.uk/101568/

Published version at: https://doi.org/10.31635/ccschem.021.202101286
Identification Number/DOI: https://doi.org/10.31635/ccschem.021.202101286
<https://doi.org/10.31635/ccschem.021.202101286>

Publisher: Chinese Chemical Society

CCS Chemistry

MINI REVIEW

Received: July 6, 2021 | Accepted: Aug. 20, 2021 | Published: Dec. 13, 2021

Whither Second-Sphere Coordination?

Wenqi Liu[1], Partha J. Das[1], Howard M. Colquhoun[2]* & J. Fraser Stoddart[1,3,4,5]*

[1]*Department of Chemistry, Northwestern University, Evanston, IL 60208,* [2]*Department of Chemistry, University of Reading, Reading RG6 6DX,* [3]*School of Chemistry, University of New South Wales, Sydney, NSW 2052,* [4]*Department of Chemistry, Stoddart Institute of Molecular Science, Zhejiang University, Hangzhou 310027,* [5]*ZJU-Hangzhou Global Scientific and Technological Innovation Center, Hangzhou 311215*

**Corresponding authors: h.m.colquhoun@rdg.ac.uk; stoddart@northwestern.edu*

Cite this: *CCS Chem.* **2022**, 4, 755–784
DOI: 10.31635/ccschem.021.202101286

The properties of coordination complexes are dictated by both the metals and the ligands. The use of molecular receptors as second-sphere ligands enables significant modulation of the chemical and physical properties of coordination complexes. In this minireview, we highlight recent advances in functional systems based on molecular receptors as second-sphere coordination ligands, as applied in molecular recognition, synthesis of mechanically interlocked molecules, separation of metals, catalysis, and biomolecular chemistry. These functional systems demonstrate that second-sphere coordination is an emerging and very promising strategy for addressing societal challenges in health, energy, and the environment.

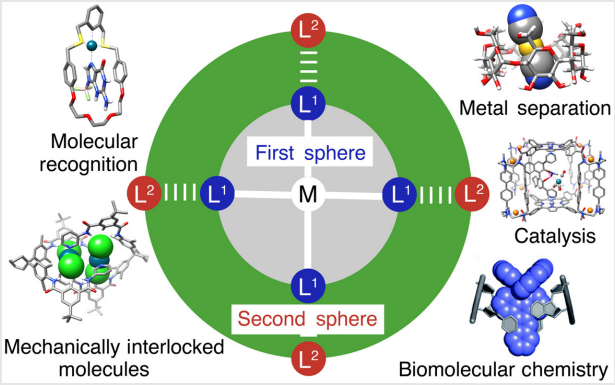

Keywords: **catalysis, coordination complexes, mechanically interlocked molecules, metal recovery, molecular recognition, supramolecular chemistry**

Introduction

Coordination chemistry,[1] the investigation of linking ligands directly to a central atom—most often a metal center—is at the heart of modern inorganic, organic, and materials chemistry. The specific combinations of ligands and metals dictate the structures and properties of the resulting coordination complexes, which are applied in numerous technologies, including metal–organic frameworks (MOFs),[2–16] optical and magnetic materials,[17,18] catalysis,[19,20] and biomedical theranostics.[21–24] In the resulting coordination complexes, the ligands linked directly to the metal center are referred to (Figure 1) as the first sphere of coordination for the metal.[25–28] Meanwhile, another set of ligands can bind to the first-sphere ligands of the coordination complex through noncovalent bonding interactions, leading to second-sphere adducts. Thus, second-sphere coordination of metal centers affords adducts that are essentially complexes of complexes.

The concept of second-sphere coordination (Figure 1c) was advanced in the first instance by Chemistry Nobel Prize Laureate Alfred Werner[29,30] in 1913. He showed that this concept could explain a number of experimental observations that could not be understood solely on the basis of first-sphere coordination.[29] These observations included (1) the formation of adducts between amines and coordinatively saturated complexes such as $[M(acac)_3]^{n+}$, (2) the presence of solvents in the crystal structures of many coordination complexes, and (3) the solvent and counterion-dependent properties associated with the optical rotations of chiral coordination complexes.

DOI: 10.31635/ccschem.021.202101286
Corrected Citation: *CCS Chem.* **2022**, 4, 755–784
Previous Citation: *CCS Chem.* **2021**, 3, 3436–3465
Link to VoR: https://doi.org/10.31635/ccschem.021.202101286

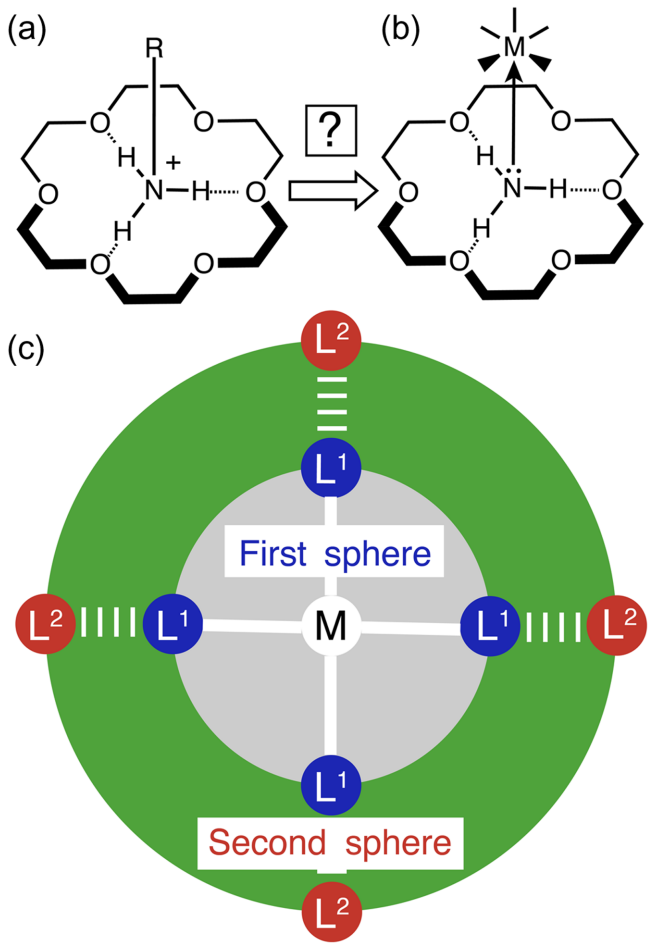

Figure 1 | *Structural formulas depicting the similarity of the three-point binding models for (a) a primary alkyammonium ion [RNH$_3$]$^+$ and (b) a transition-metal ammine. (c) Graphical representation of the concept of second-sphere coordination. A transition metal (M) is coordinated with first-sphere ligands L^1, which interact with second-sphere ligands L^2 through noncovalent bonding interactions. Adapted with permission from ref 35. Copyright 1983 Royal Society of Chemistry.*

Beginning in the early 1980s, we sought to gain insight into the nature of second-sphere coordination by investigating the interactions between transition-metal complexes and synthetic molecular receptors.[31] Crown ethers are well-known to form complexes with primary alkylammonium ions, [RNH$_3$]$^+$, through hydrogen bonding and ion-dipole interactions.[32–34] It occurred to us that the geometric and electronic (stereoelectronic) features of an [RNH$_3$]$^+$ ion closely resemble (Figures 1a and 1b) those of a transition-metal ammine complex,[35] [ML$_x$(NH$_3$)]$^{n+}$. The recognition of this similarity led to our initial investigations of crown ether receptors as second-sphere ligands, resulting in the isolation of a novel series of adducts between crown ethers and transition-metal complexes,[36–39] whose superstructures were quickly established by X-ray crystallography. Figure 2 presents a collage [(a)–(s)] of some of the solid-state superstructures that are reproduced from a review[25] that was published in *Angewandte Chemie* on "Second-Sphere Coordination—A Novel Rôle for Molecular Receptors" in 1986. The review was the first one to be published in the chemical literature with a copious use of color: at that time, it cost us the equivalent of £10,000. One of the most remarkable examples (Figures 2j and 2k) was the 1:1 adduct formed[38] between dibenzo[30]crown-10 (DB30C10) and [Pt(bpy)(NH$_3$)$_2$]$^{2+}$. The fascinating feature of this superstructure is that, in addition to the three pairs of [N–H···O] hydrogen bonds between the oxygen atoms in the crown ether and the hydrogen atoms of the NH$_3$ ligands, there are close, complementary [π···π] stacking (charge transfer) interactions between the two π-electron-rich aromatic (catechol) rings in the receptor molecule and the π-electron-poor 2,2′-bipyridine ligand in the platinum-based substrate. This second-sphere coordination adduct was shown by ^{1}H NMR spectroscopy to exist as a stable complex in solution as well as in the solid state.[38] The high stability of this adduct is sustained by multiple weak interactions between the receptor and the ligands on the transition-metal complex. In contrast, conventional second-sphere ligands, such as water or alcohols, only form weak adducts with metal complexes through monovalent binding, and the well-defined superstructures observed crystallographically in the solid state are not sustained in solution. For example, in the crystal superstructure[38] of a lanthanum complex [La(tptz)(NO$_3$)$_3$(H$_2$O)]•2C$_2$H$_5$OH, the two ethanol molecules form hydrogen bonds with the coordinated H$_2$O molecule. Although the solid-state superstructure is well-defined, there is no suggestion that it exists in solution. Molecular receptors, when employed as second-sphere ligands, lead to the formation of stable, robust, and predictable adducts in contrast to those adducts formed by weakly binding ligands observed only in the solid state.

It may be noted that the superstructure of the bipyridine-based second-sphere adduct shown in Figure 2 as a space-filling representation (j) and as a ball-and-stick representation (k) provided (Box 1) inspiration for subsequent research into complex formation between dibenzo-crown ethers and the dicationic bipyridinium herbicides Diquat, derived from 2,2′-bipyridine, and Paraquat, derived from 4,4′-bipyridine. The success of the latter investigation in turn led to the discovery of the tetracationic cyclophane, cyclobis(paraquat-*p*-phenylene), known as Blue Box, which has since proved a hugely valuable component in developing the field of mechanically interlocked molecules (MIMs) and eventually artificial molecular machines (AMMs).

Following our initial work on using synthetic molecular receptors to bind coordination complexes, there was a surge in the study of second-sphere coordination. Numerous macrocyclic and polycyclic crown ethers,[39–50] cyclodextrins (Figures 3a and 3b),[51–65] calixarenes

DOI: 10.31635/ccschem.021.202101286
Corrected Citation: *CCS Chem.* **2022**, 4, 755–784
Previous Citation: *CCS Chem.* **2021**, 3, 3436–3465
Link to VoR: https://doi.org/10.31635/ccschem.021.202101286

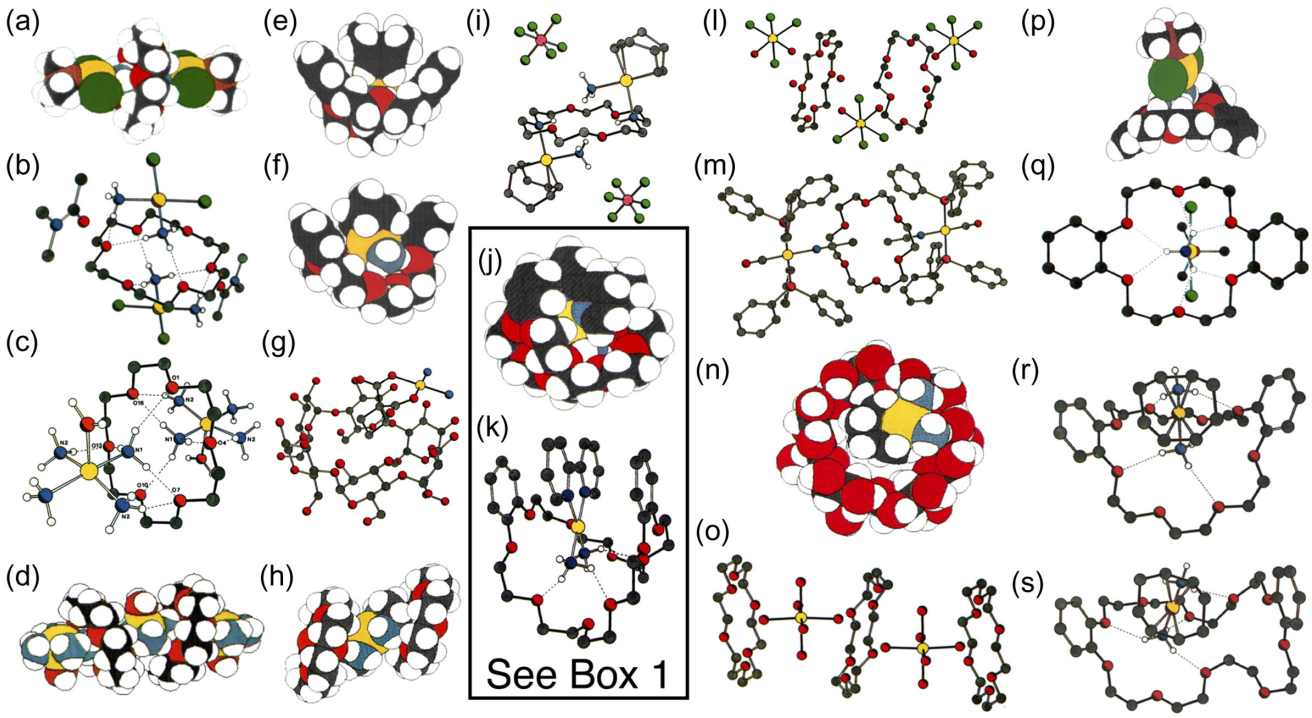

Figure 2 | *A sampling of solid-state superstructures of 1:1 adducts between transition-metal complexes and macrocyclic receptors taken directly from the 1986 review on second-sphere coordination published in Angewandte Chemie, where the superstructures are presented with space-filling or ball-and-stick models for (a) [{trans-Pt(PMe$_3$)Cl$_2$(NH$_3$)}$_2$•l8C6]; (b) [{cis-Pt(NH$_3$)$_2$Cl$_2$•dma}$_2$•l8C6]; (c and d) [Cu(NH$_3$)$_4$(H$_2$O)•18C6]$_n^{2n+}$; (e) [Rh(cod)(NH$_3$)$_2$•DB21C7]$^+$; (f) [Rh(nbd)(NH$_3$)$_2$•DB24C8]$^+$; (g) [diammine-1,1-cyclobutanecarboxylatoplatinum(II)-α-CD]; (h) [Pt(en)$_2$•18C6]$_n^{2n+}$; (i) diamminebis-(1,5-cyclooctadiene)(μ-l,4-l0,l3-tetraoxa-7,l6-diazacyclooctadecane-N^7,N^{16})-dirhodium bis(hexafluorophosphate); (j and k) [Pt(bpy)(NH$_3$)$_2$•DB30C10]$^{2+}$; (l) [SnCl$_4$(H$_2$O)$_2$•18C6][H$_2$O]$_2$; (m) [{trans-Ir(CO)(CH$_3$CN)(PPh$_3$)$_2$}$_2$•18C6]$^{2+}$; (n) [Rh(cod)(NH$_3$)$_2$•α-CD]$^+$; (o) [Mn(H$_2$O)$_6$•18C6]$_n^{n+}$ (ClO$_4^-$ salt); (p and q) [trans-Pt(PMe$_3$)Cl$_2$(NH$_3$)•DB18C6]; (r) [Rh(cod)(NH$_3$)$_2$•DB24C8]$^+$; (s) [Rh(cod)(NH$_3$)$_2$•DB30C10]$^+$. The X-ray superstructure (j and k) of [Pt(bpy)(NH$_3$)$_2$•DB30C10]$^{2+}$ inside the highlighted rectangle will be discussed in Box 1. Adapted with permission from ref 25. Copyright 1986 John Wiley and Sons.*

(Figure 3e),[66-71] resorcinarenes (Figure 3d),[72] pillararenes (Figure 3f),[73] cucurbiturils (Figure 3c),[74] and cyclophanes[75-79] all proved to be efficient second-sphere ligands and even, in some examples, acted simultaneously as both first- and second-sphere coordination ligands (Figure 2i).[80-83] As a result, many second-sphere coordination adducts were discovered by exploiting the whole range of noncovalent bonding interactions, including hydrogen bonding, charge transfer, [π···π] stacking, hydrophobic effects, and van der Waals interactions. Summaries of these early investigations of second-sphere coordination chemistry may be found in several reviews,[25-28,84-90] published by us as well as by other groups.

Over the past two decades, there has been a resurgence of interest in second-sphere coordination. Advances in supramolecular, organic, inorganic, biomolecular, and materials chemistry have created[91,92] new demands for molecular receptors capable of binding a wide range of substrates, constructing MIMs, separating different metals, and catalyzing organic reactions. In such contexts, second-sphere coordination has emerged as a valuable strategy for solving previously intractable problems. This minireview highlights many new adducts based on molecular receptors as second-sphere coordination ligands.

Molecular Recognition

Second-sphere coordination can be applied to the design and construction of new supramolecular complexes by incorporating noncovalent binding sites into ligands, followed by their coordination to transition metals. The metal ion can participate in molecular recognition by a receptor molecule either indirectly via second-sphere coordination or directly via simultaneous first- and second-sphere coordination, targeting specific substrates by tailored receptor-substrate and metal-ligand interactions.

DOI: 10.31635/ccschem.021.202101286
Corrected Citation: *CCS Chem.* **2022**, 4, 755–784
Previous Citation: *CCS Chem.* **2021**, 3, 3436–3465
Link to VoR: https://doi.org/10.31635/ccschem.021.202101286

Box 1. | *A 40-year research trail illustrating how one observation in 1981 led to another line of research and so on—and how this dynamic is as sustained over four decades.*

(a)

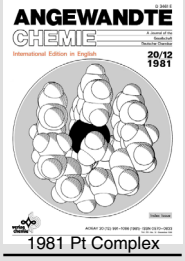

1981 Pt Complex

(b)

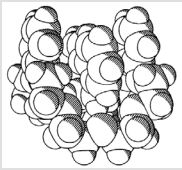

1983 Diquat

(c)

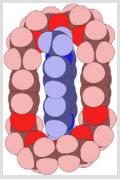

1987 Paraquat

(d)

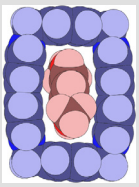

1988 Blue Box

(e)

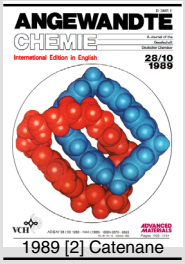

1989 [2] Catenane

(f)

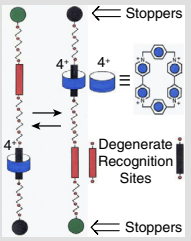

1991 Molecular Shuttle

(g)

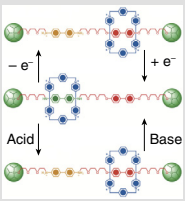

1994 Molecular Switch

In the middle of a 20-year (1970-1990) sojourn at Sheffield University, I (JFS) availed myself of the opportunity to spend a three-year period from 1978–1981 on secondment at the ICI Corporate Laboratory in Runcorn, Cheshire in the United Kingdom. There, I met Howard Colquhoun and together we asked ourselves the question — would transition metal complexes (TMCs) with ammine ligands bind to crown ethers (CEs)? The answer was a resounding yes, so much so that we became very quickly involved in an intensive program of research relating to the adducts formed between TMCs and CEs. One of these 1:1 adducts — which was to grace (a) the front cover of *Angewandte Chemie* in black-and-white in 1981 — between $Pt(bipy)(NH_3)_2^{2+}$ and dibenzo[30]crown-10 (DB30C10) caught our attention because of the donor-acceptor interactions — reflected in the yellow color of the adduct in acetonitrile solution — between the π-electron rich catechol rings on the CE and the π-electron deficient bipyridine ligand coordinated to the Pt-metal center. At the time, Imperial Chemical Industries (ICI) was marketing a 1:1 mixture of Diquat and Paraquat worldwide as a wipe-out weed killer and so we asked ourselves the obvious question — would DB30C10 form a 1:1 complex with Diquat and (b) it did! The next question we faced was — which CE would form a 1:1 complex with Paraquat? The answer, which was far too long in coming, was a constitutional isomer of DB30C10 — namely, bisparaphenylene[34]crown-10 (BPP34C10) which was shown (c) in 1987 to form a 1:1 complex with Paraquat. We had put blue inside red: now we had to put red inside blue — a goal which sent us in the direction of synthesizing cyclobis(paraquat-p-phenylene) ($CBPQT^{4+}$ or the little blue box) in 1988: its 1:1 complex with 1,4-dimethoxybenzene was published (d) in two back-to-back communications in *Angewandte Chemie* in 1988. The template-directed synthesis of the first (e) donor-acceptor [2]catenane followed hard on the heels of these two communications, on this occasion being granted front-cover status on the October issue of *Angewandte Chemie* in 1989. On 1 June, 1991 our first (f) molecular shuttle — a degenerate [2]rotaxane with two π-donating hydroquinone recognition sites for the $CBPQT^{4+}$ ring on the rod component of a dumbbell — was published in the *Journal of The American Chemical Society*. A non-degenerate counterpart, which can be switched (g) either chemically or electrochemically and incorporating benzidine and biphenyl recognition sites for the $CBPQT^{4+}$ ring, was described in *Nature* in 1994. In the same year, we reported the template-directed synthesis of a [5]catenane, also known as (h) Olympiadane, and three years later in 1997 published in a communication, (i) a branched [7]catenane, both appearing in *Angewandte Chemie*. In 2000, a bistable [2]catenane, in which the CE ring incorporates a tetrathiafulvalene (TTF) and a 1,5-dioxynaphthalene (DNP) unit was introduced into a molecular switch tunnel junction (MSTJ) and (j) reported in *Science*, along with its mechanically interlocked $CBPQT^{4+}$ ring. A bistable [2]rotaxane, in which the $CBPQT^{4+}$ ring undergoes redox-promoted switching between TTF and DNP units was used in 2007 to create a 160-kbit memory at a density of 10^{11} bits per square centimeter: this milestone (k) in molecular electronics was announced in *Nature*. In 2010, we described an intellectually disruptive discovery in *Nature Chemistry*. The ability of $CBPQT^{4+}$ ring, when reduced to its bisradical dication ($CBPQT^{2\bullet+}$) to form (l) a strong 1:1 trisradical tricationic complex with methyl viologen radical cation, led to the design and synthesis of a pumping cassette, based on 3,5-dimethylpyridinium, bipyridinium and isopropylphenylene units. The pumping cassette was subsequently to serve as a key component in the operation of a (m) molecular pump, described in *Nature Nanotechnology* in 2015, and a (n) polyrotaxane synthesizer, published in *Science* in 2020.

The observation of donor-acceptor interactions in a 1:1 adduct formed between a transition metal ammine carrying a bipyridine ligand and a crown ether containing a couple of catechol units led to a sequence of events during four decades that could have not been foreseen in 1981, yet can be recalled and rationalized in 2021, such is the nature of research when its progress is left to its own devices with minimum intervention on the part of others, with the exception of countless collaborators whose involvement was scientifically driven.

(h)

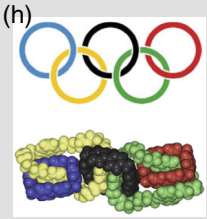

1994 Olympdane

(i)

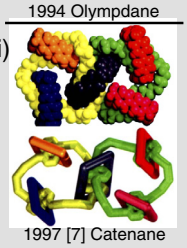

1997 [7] Catenane

(j)

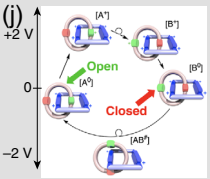

2000 Molecular Electronics

(k)

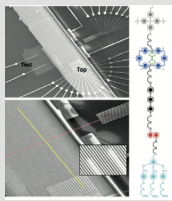

2007 160 Kbit Memory

(l)

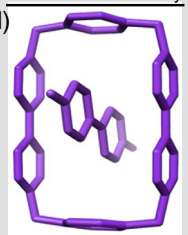

2010 Trisradical Complex

(m)

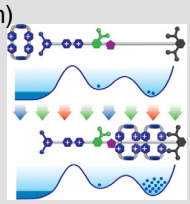

2015 Molecular Pump

(n)

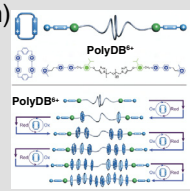

2020 Polyrotaxane Synthesizer

DOI: 10.31635/ccschem.021.202101286
Corrected Citation: *CCS Chem.* **2022**, 4, 755–784
Previous Citation: *CCS Chem.* **2021**, 3, 3436–3465
Link to VoR: https://doi.org/10.31635/ccschem.021.202101286

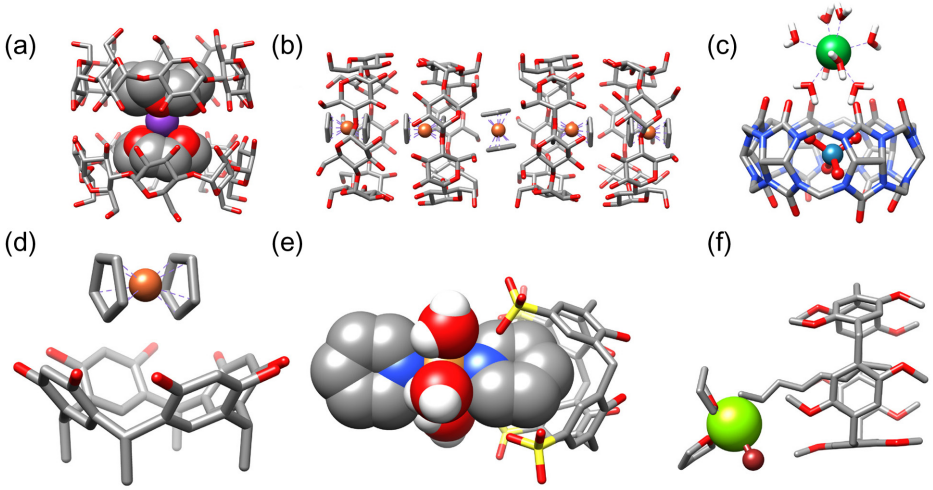

Figure 3 | *Representative examples of solid-state superstructures for second-sphere coordination adducts reported by other researchers. (a) Tubular and space-filling representation of a 2:2:1 adduct of γ-cyclodextrin•12-crown-4•K^+. (b) Tubular and space-filling representation of a 4:5 adduct of β-cyclodextrin•ferrocene. (c) Tubular and ball-and-stick representation of a 1:1 adduct of cucurbit[6]uril•$[Yb(OH_2)_8]^{3+}[ReO_4]^-$. (d) Tubular and space-filling representation of a 1:1 adduct of resorcinarene•ferrocene. (e) Tubular and space-filling representation of a 1:1 adduct of $[Cu(NC_5H_5)_2(H_2O)_4$•calix[4]arene sulfonate]. (f) Tubular and space-filling representation of a 1:1 adduct of (n-octyl)$MgBr(THF)_2$•pillar[5]arene.*

Loeb et al.[50,80–83,93,94] have demonstrated the design and synthesis of several molecular receptors that interact with substrates through second-sphere interactions. One example involves[80,94] a family of thiacyclophane receptors that recognize DNA nucleobases. The molecular recognition displayed by these receptors involves several different types of interaction, including (1) first-sphere coordination from a N atom of the nucleobase substrate to a Pd(II) metal center, (2) second-sphere hydrogen bonding between a NH_2 group of the substrate and polyether O atoms of the receptors, and (3) [π···π] stacking between the π-electron-rich aromatic spacing units of the receptors and the π-electron-poor aromatic rings of the substrates. Single-crystal X-ray analyses of two adducts involving a receptor binding either with adenine or guanine—the latter as a BF_3 adduct—reveals that all three interactions mentioned above exist in these adducts with near-ideal interaction parameters (Figures 4a and 4c). The molecular recognition of cytosine was realized by a receptor having coordination sites for Pd(II) and polyether functional groups. Single-crystal X-ray analysis (Figure 4b) reveals that adduct formation between this receptor and cytosine is sustained by direct first-sphere coordination from a N atom of cytosine to the Pd(II) metal center, aided and abetted by hydrogen-bonding interactions between the NH_2 group of cytosine and polyether O atoms of the macrocyclic receptor. These adducts between the DNA nucleobases and their receptors have been proved to exist both in the solid state and in solution. The same principles have been applied[81–83] in designing synthetic receptors for molecular recognition of other substrates, including barbiturates, amino acids, amines, and hydrazinium ions.

Huc et al.[95–98] have presented (Figure 5a) the chemical community with several examples of molecular recognition through second-sphere coordination using molecular capsules formed by metal-coordination-directed folding of a helical oligomer. A key chain segment,

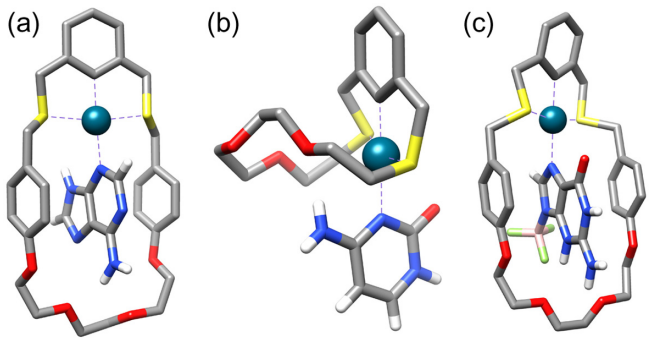

Figure 4 | *Stick representations of the X-ray superstructures of thiacyclophane receptors complexed with (a) adenine, (b) cytosine, and (c) guanine (BF_3) through a combination of several interactions, including (1) first-sphere coordination from N atoms to Pd(II) metal center, (2) second-sphere hydrogen bonds between the NH_2 group of the substrate and polyether O atoms of the receptors, and (3) [π–π] stacking between the electron-rich aromatic spacing units of the receptors and the electron-poor aromatic rings of the substrates.*

DOI: 10.31635/ccschem.021.202101286
Corrected Citation: *CCS Chem.* **2022**, 4, 755–784
Previous Citation: *CCS Chem.* **2021**, 3, 3436–3465
Link to VoR: https://doi.org/10.31635/ccschem.021.202101286

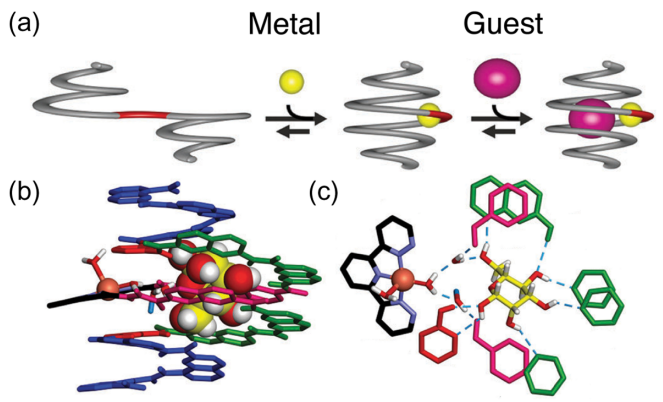

Figure 5 | *(a) Schematic illustration of molecular recognition through second-sphere coordination using helical molecular capsules formed by metal-coordination-directed folding. (b) Stick-and-sphere representation of X-ray crystal superstructure of an adduct between a β-D-mannopyranose and a helical foldamer ligand associated with Cu^{2+}. (c) A zoomed-in view of the substrate associated with the capsule through second-sphere coordination, which involves hydrogen-bond (dashed lines) formation between the foldamer ligand and the hydroxyl groups of the β-D-mannopyranose. The Cu^{2+} center adopts a square pyramidal geometry, coordinating with three nitrogen atoms of the pyz–pyr–pyz segment and two O atoms of two H_2O molecules. Adapted with permission from ref 97. Copyright 2018 Royal Society of Chemistry.*

pyridazine–pyridine–pyridazine (pyz–pyr–pyz), was introduced into the oligomer.[95] This segment exists in an *anti–anti* conformation that is favored by repulsion between the endocyclic N atoms, directing the oligomer into an extended conformation instead of a capsular shape. As a result, this oligomer displays no propensity for molecular recognition in the absence of metal ions. Coordination of transition-metal ions Cu^+, Cu^{2+}, and Ag^+, as well as the alkali metal ions Na^+ and K^+, induces folding of the oligomer into a capsular shape by favoring a *syn–syn* conformation for the pyz–pyr–pyz segment.[96] In all cases, the metal ions were positioned on one side of the cavity wall, leaving its coordination sphere occupied partially by solvent molecules and available to bind a guest. The first-sphere coordination between guests and the metal centers can enhance the binding affinity of the helix, while the second-sphere interaction between the guest and the inner wall of the capsule leads to shape and size selectivity. Moreover, interaction of the oligomer with a hydrated Ca^{2+} or Ba^{2+} ion occurs *entirely* in the second sphere, via hydrogen bonding between ion-coordinated water and oligomeric N atoms, but still results[95] in a helical geometry for the oligomeric complex.

As an extension of these earlier reports, the same authors demonstrated molecular recognition of carbohydrates[97] in organic solvents using foldamer-type molecular capsules, by taking advantage of first- and second-sphere coordination. Depending on the nature of the metal center, the molecular capsules show different binding affinities and diastereoselectivities toward a range of carbohydrates, including D/L-threitol, xylitol, D/L-mannopyranose, D/L-glucopyranose, D/L-galactopyranose, and D/L-fructopyranose. For example, the Cu^{2+} complex of the foldamer binds D-threitol 14 times more strongly than its K^+ counterpart. X-Ray crystal superstructure analysis of the adducts between a Cu^{2+}-coordinated capsule and D/L-mannopyranose reveals (Figures 5b and 5c) that the substrate is associated with the capsule through second-sphere coordination, which involves hydrogen bond formation between the foldamer ligand and the hydroxy groups of the mannopyranose. The Cu^{2+} center adopts a square pyramidal geometry, coordinating with three N atoms of the pyz–pyr–pyz segment and the O atoms of two H_2O molecules. The D-mannopyranose assumes the β-pyranose configuration in the solid state. In contrast, this molecule exists predominantly (97%) in the α-pyranose form in $CHCl_3/Me_2SO$ (4:1, v/v) solution. The authors also reported the single-crystal superstructure of an adduct between D/L-threitol and a smaller analog of the molecular capsule coordinated with a Cu^{2+} ion. Here, the Cu^{2+} center interacts with the substrate through second-sphere coordination involving solvents—a H_2O and a MeOH molecule—that are coordinated directly to the metal ion. As an extension of such molecular recognition, the authors also developed a new strategy[98] to prepare the foldamer capsule shells around a [2Fe–2S] cluster. The foldamer shell influences the structural and spectroscopic properties of the metal cluster, including desymmetrization and confinement of part of its first coordination sphere within the foldamer cavity.

Leigh et al.[99–102] have reported molecular recognition of chloride anions through second-sphere coordination using molecular knots. These molecular knots were synthesized (Figure 6a) by transmetallation of a Zn(II) infused pentafoil (5_1) knot with tetrafluoroborate salts of Co(II), Cu(II), and Ni(II).[99] The resulting metallated knots exhibit second-sphere coordination of a single chloride anion within the central cavity of the knot by utilizing both multiple [CH···Cl^-] hydrogen bonds and electrostatic interactions. X-ray crystal superstructures of these transmetallated pentafoil knots reveal (Figures 6b–6d) that five of the 15 bipyridine groups form an inner cavity lined with 10 electron-poor H atoms that form an array of hydrogen bonds with the chloride anion located inside the cavity. This type of second-sphere coordination is the first example exhibited in molecular-knot geometry. The diameter of the central cavity varies depending on the metal cation: 3.3 Å for Fe(II), Zn(II), and Ni(II), and 3.5 Å for Co(II). The metal-to-metal distance in the distorted cobalt knot is, however, smaller than those in the case of iron, nickel, and

DOI: 10.31635/ccschem.021.202101286
Corrected Citation: *CCS Chem.* **2022**, 4, 755–784
Previous Citation: *CCS Chem.* **2021**, 3, 3436–3465
Link to VoR: https://doi.org/10.31635/ccschem.021.202101286

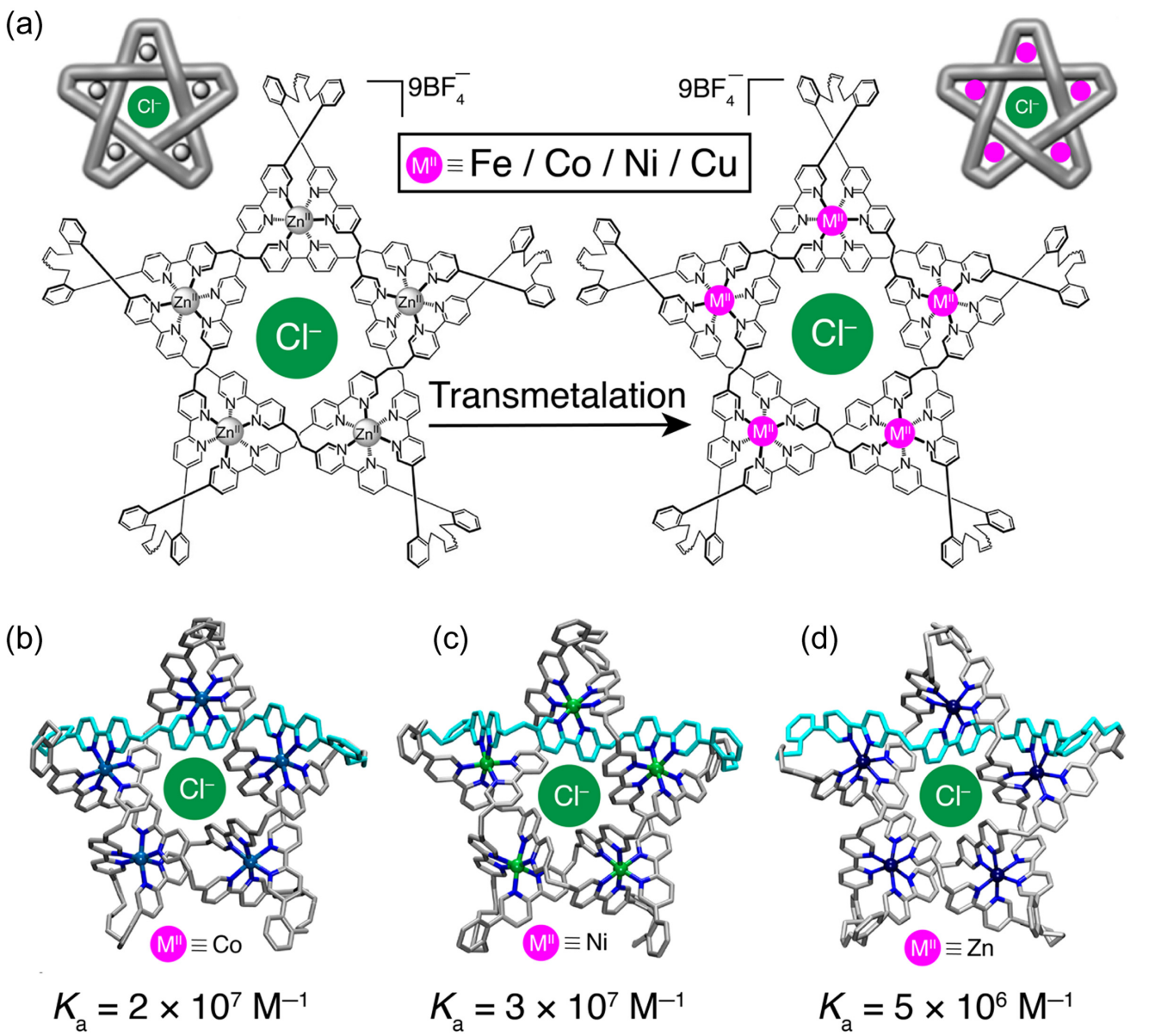

Figure 6 | *(a) Graphical illustration and structural formulas of various pentafoil knotted complexes synthesized by transmetalation of Zn(II) infused pentafoil (5_1) knot with tetrafluoroborate salts of Co(II), Cu(II), and Ni(II). The resulting metallated knots exhibit second-sphere coordination of a single chloride ion within the central cavity of the knot, providing [CH···Cl⁻] hydrogen bonding and electrostatic interactions. (b) Ball-and-stick representations of the X-ray crystal superstructures of chloride complex using the pentafoil knots sustained by the coordination with (b) Co^{2+}, (c) Ni^{2+}, and (d) Zn^{2+}. The binding affinities for Cl^- anions are determined by the second-sphere coordination and electrostatic interactions with different M(II) ions.*

zinc pentafoil knots. In contrast, the metal–metal–metal *angle* is higher in cobalt compared with those in the other three metallic pentafoil knots. These conformational changes in the knotted ligands lead to different distances between the chloride anion and the metal ions in these knot complexes. As a result, the binding affinities for chloride anion through second-sphere coordination and electrostatic interaction vary with different M(II) ions over nearly three orders of magnitude, from K_a = 8 × 10^4 M^{-1} (Cu^{2+} knot) to K_a = 3.3 × 10^7 M^{-1} (Fe^{2+} knot) in MeCN.

Construction of Mechanically Interlocked Molecules

The synthesis of MIMs[103–108] such as catenanes,[109–122] rotaxanes,[123–132] and suitanes[133–139] has become a field with intense research activity on account of the potential of such molecules to act as molecular machines.[140–153] Several effective synthetic strategies for synthesizing MIMs have been achieved, based on the template effect.[154–156]

DOI: 10.31635/ccschem.021.202101286
Corrected Citation: *CCS Chem.* **2022**, 4, 755–784
Previous Citation: *CCS Chem.* **2021**, 3, 3436–3465
Link to VoR: https://doi.org/10.31635/ccschem.021.202101286

One of these strategies involves the coordination of organic ligands to transition metals to promote the formation of mechanically interlocked structures.[157–168] Second-sphere coordination, as an extension of this strategy, can also be employed to advance the effective synthesis of MIMs. Wisner et al.[169–173] demonstrated the use of second-sphere coordination to prepare several MIMs such as rotaxanes and catenanes. For example, this group described the synthesis of [2]pseudorotaxanes in a single step employing second-sphere coordination.[169] An isophthalamide-based tetralactam macrocycle, serving as the second-sphere ligand, establishes four sets of hydrogen bonds with the two chloride first-sphere ligands in a *trans*-palladium dichloride complex, leading to formation of a pseudorotaxane. It was found that the stability of the pseudorotaxane diminishes markedly as the size of the halide ligand increases from Cl < Br < I. In a subsequent investigation, these authors reported[170] the synthesis of a [2]rotaxane based on the same system. To produce the mechanically interlocked architecture shown in Figure 7a, 4-(3,5-di-*tert*-butylbenzyloxy)-pyridine was employed as the ligand, on the basis that its terminal groups are sterically demanding and function as stoppers to prevent the dethreading of the tetralactam macrocycle. The rotaxane was obtained in 89% isolated yield simply by mixing the tetralactam macrocycle, the ligands, and *trans*-bis(benzonitrile)palladium(II) dichloride in $CHCl_3$ at room temperature. The resulting rotaxane is soluble in $CHCl_3$ and remains stable over time as well as under column chromatographic conditions. The structure of the rotaxane was confirmed by X-ray crystallographic analysis, which revealed (Figure 7b) that the amide groups of the isophthalamide subunits in the macrocycle establish four sets of hydrogen bonds with the chloride ligands of the palladium(II) metal complex, providing the driving force for rotaxane formation. Following these investigations, these same authors explored[172] the stabilities of a series of pseudorotaxanes by varying the metals and the *para*-substituted pyridine ligand. They found that the hydrogen bond-accepting ability of the chloride ligands can be tuned by varying the electron-donating/-withdrawing nature of the *para*-substituted pyridine coligands. Moreover, the stability of the pseudorotaxane in $CHCl_3$ solution decreases slightly when the Pd(II) ion is replaced by Pt(II). Replacing chloride by thiocyanate in the first coordination sphere led to the formation (Figure 7c) of a series of (pseudo)rotaxanes by second-sphere coordination (hydrogen bonding) between the thiocyanate ligands and the amide units of the macrocycle.[171] The directional nature of the thiocyanate ligands affords a doubly degenerate binding geometry, leading to a rotaxane (Figure 7c) in which the ring shuttles back and forth 3300 times a second in solution at 15 °C.

In another example, Wisner et al.[173] demonstrated the construction of catenanes (Figure 8a) using simultaneous first- and second-sphere coordination. An acyclic bidentate ligand that resembles a three-quarter unit of a previously employed tetralactam macrocycle was designed and synthesized. This ligand coordinates directly to a $PdCl_2$ unit in a *trans* arrangement, and the resulting product comprises (Figure 8a) a pair of catenated macrocycles, each incorporating the metal subunit *trans*-$PdCl_2L_2$ in its scaffold. The catenation is driven by mutual recognition of the $PdCl_2L_2$ subunit in one ring by its orthogonally positioned partner. The catenane was synthesized in 87% isolated yield simply by heating a solution of an equimolar amount of $Pd(PhCN)_2Cl_2$ and the *trans*-bidentate ligand. X-ray crystallographic analysis of the catenane reveals (Figure 8b) that a template effect is manifested in the interaction between both the $PdCl_2$ subunits and their opposing macrocyclic cavities. Eight pairs of [NH···Cl] hydrogen bonds were found between the first-sphere Cl^- ligands and the amide units of the second-sphere ligand. A reversible transformation between catenane and macrocycle was also demonstrated by varying the solvent polarity. Transformation of the catenane into two individual macrocycles was observed when the sample was dissolved in the mixed solvent system $(CD_3)_2SO/CDCl_3$ as a result of competitive binding of the polar solvent with the NH groups of the macrocycle. The catenane re-forms when the macrocycle is redissolved in $CDCl_3$.

Metal Separation

Second-sphere coordination of transition-metal complexes could lead to changes in solubility of the resulting adducts, which can be utilized for the separation of metal ions. We demonstrated (Figure 9c) the separation of copper from cobalt using[35] this principle in 1983. We found that 18C6 formed (Figure 9a) a 1:1 polymeric adduct with $[Cu(NH_3)_4(H_2O)][PF_6]_2$, leading to precipitation from aqueous solution. X-ray structural investigation revealed that each macrocycle is involved in no fewer than 10 hydrogen bonds with the ammine ligands. A similar adduct obtained (Figure 9b) from the cobalt(III) complex $[Co(NH_3)_6][PF_6]_3$, requires the addition of a two-molar excess of 18C6 to its aqueous solution in order to form a crystalline orange precipitate. When one molar equivalent of 18C6 was added to a solution containing one molar equivalent of each of $[Co(NH_3)_6][PF_6]_3$ and $[Cu(NH_3)_4(H_2O)][PF_6]_2$, the 1:1 copper adduct was precipitated exclusively in >90% yield. A simple filtration separated the precipitated copper adduct from the cobalt-containing solution. The 18C6 ligand was recovered by treating the 1:1 adduct with HCl solution, yielding aqueous copper(II) and insoluble $[NH_4][PF_6]$•18C6. The ammonium hexafluorophosphate adduct with 18C6

DOI: 10.31635/ccschem.021.202101286
Corrected Citation: *CCS Chem.* **2022**, 4, 755–784
Previous Citation: *CCS Chem.* **2021**, 3, 3436–3465
Link to VoR: https://doi.org/10.31635/ccschem.021.202101286

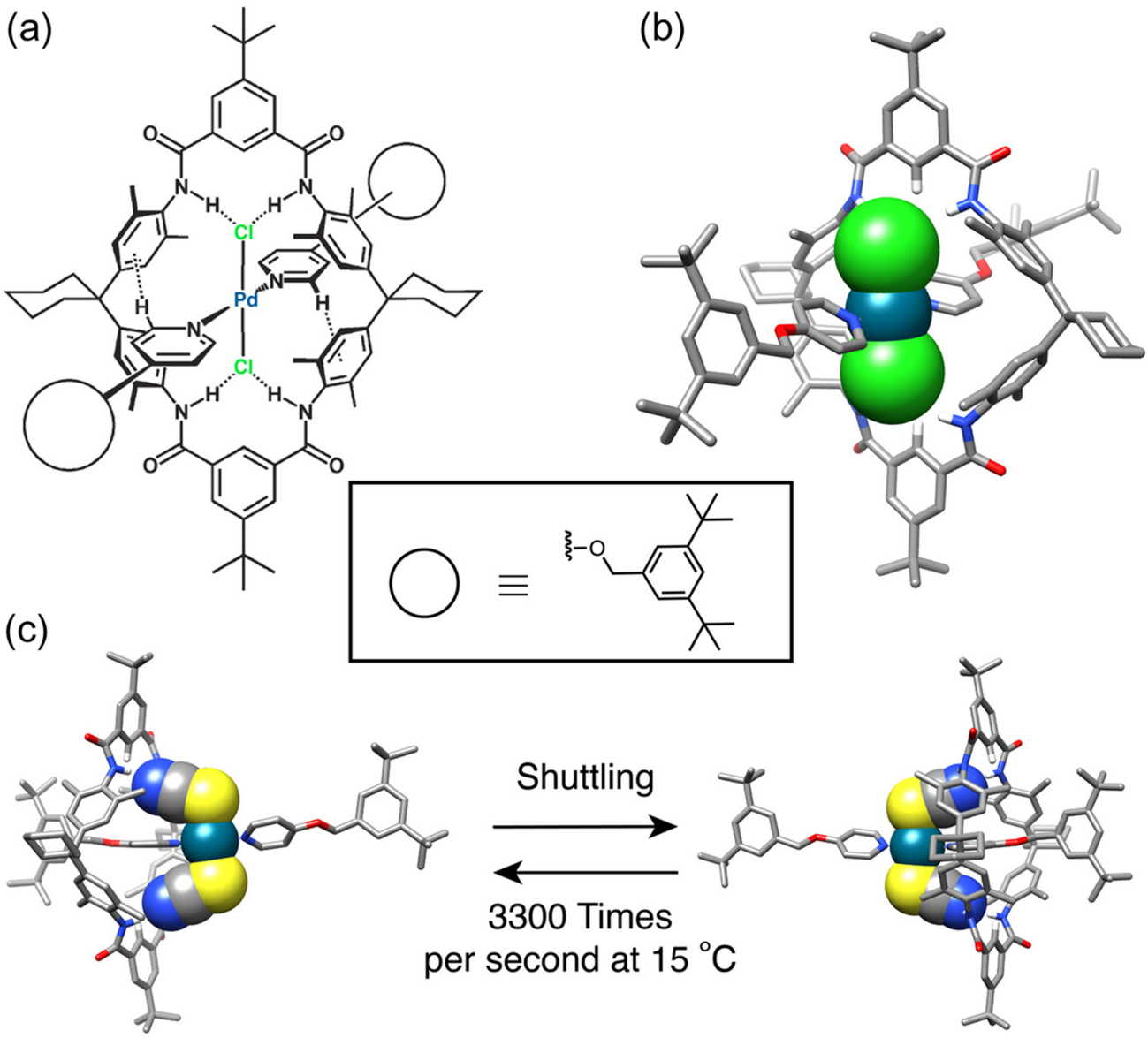

Figure 7 | *(a) Structural formula and (b) tubular and space-filling representations of X-ray solid-state superstructure of a rotaxane constructed by second-sphere coordination. The amide groups of the isophthalamide subunits in the macrocycle establish four sets of hydrogen bonds with the chloride ligands of the palladium(II) metal complex, providing the driving force for the [2]rotaxane formation. (c) X-ray solid-state structure of a [2]rotaxane formed by second-sphere coordination between the thiocyanate ligands and the amide units of the macrocycle. The directional nature of the thiocyanate ligands affords a degenerate binding geometry, leading to a degenerate [2]rotaxane shuttle where the ring moves back and forth along the dumb-bell shaped axle 3300 times a second in $CDCl_3$ solution at 15 °C. Adapted with permission from ref 170. Copyright 2006 Royal Society of Chemistry.*

could be used again in separating $[Cu(NH_3)_4(H_2O)]^{2+}$ from $[Co(NH_3)_6]^{3+}$.

In a similar fashion, just as ammine ligands on transition metals bind to crown ethers, aqua ligands coordinate[25] to electropositive metals through oxygen $[M{\leftarrow}OH_2]^{n+}$, showing an enhanced dipole and increased acidity of the ligand. Crown ethers,[25,174] macrocyclic polyamines,[175] and acyclic trisulfonate ligands[176–178] have all been reported as receptors for aqua complexes of Mn^{3+}, Co^{2+}, Th^{4+}, U^{4+}, Sn^{4+}, Er^{3+}, and so on. The resulting adducts show different solubilities and propensities for crystallization, properties that can be utilized for metal separation. Shimizu et al.[176] have shown (Figure 10) that 1,3,5-tris(sulfomethyl)benzene trianions can be employed as second-sphere ligands for aqua complexes. The methylsulfonate groups on this ligand adopt a *cis–cis–cis* orientation, that is, they are all on the same side of the benzene core. The convergently oriented

DOI: 10.31635/ccschem.021.202101286
Corrected Citation: *CCS Chem.* **2022**, 4, 755–784
Previous Citation: *CCS Chem.* **2021**, 3, 3436–3465
Link to VoR: https://doi.org/10.31635/ccschem.021.202101286

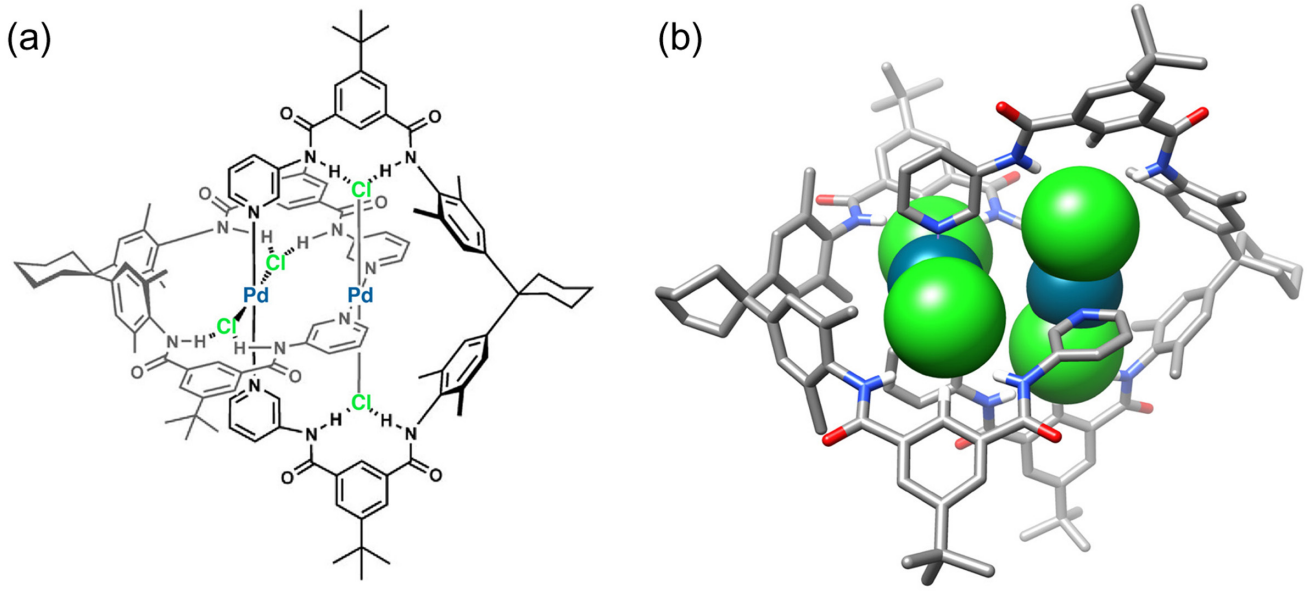

Figure 8 | *(a) Structural formula and (b) tubular and space-filling representations of X-ray solid-state structure of a catenane constructed by second-sphere coordination. The catenation formation is driven by the mutual recognition of the $PdCl_2L_2$ subunit in one ring by its orthogonally disposed partner. Eight pairs of [NH···Cl] hydrogen bonds were found between the first-sphere Cl ligands and the amide units of the second-sphere ligand. Adapted with permission from ref 173. Copyright 2007 John Wiley and Sons.*

sulfonate groups interact with aqua ligands through hydrogen bonds. The authors found[177,178] that trivalent cations (Fe^{3+}, Cr^{3+}, and Al^{3+}) can be sandwiched (Figures 10a–10c) between two of the ligands, forming 1:2 adducts. Each ligand participants in the formation of six hydrogen bonds with the aqua ligands. This trisulfonate ligand also forms (Figures 10d–10f) 1:1 adducts when divalent cations (Cu^{2+}, Mg^{2+}, and Zn^{2+}) are used. The 1:2 adducts, however, showed a better propensity to form crystals. Competitive crystallization was performed when equal molar amounts of the ligand, $Fe(NO_3)_3$, and $Zn(NO_3)_2$ were combined in an aqueous solution. Diffusion of MeOH into this mixture afforded only yellow crystals of the 1:1 adduct between the ligand and Fe^{3+} aqua complex, leaving all the Zn^{2+} in solution. This group also has demonstrated[179–181] the construction of porous materials by embracing second-sphere coordination to aqua ligands.

One of the most commercially successful processes for gold mining involves the cyanide protocol. A critical step in this protocol is to strip $Au(CN)_2^-$ ions from the surface of carbon into an aqueous solution under harsh conditions,[182–184] involving high temperatures (95–140 °C), high pressures (70–400 kbar), and concentrated solutions of cyanide and hydroxide. There is a demand to develop new technologies that allow the operation of this protocol to occur under much milder conditions. We have, at Northwestern University (NU), demonstrated[185] that second-sphere coordination between α-cyclodextrin (α-CD) and $KAu(CN)_2$ can be used to facilitate the separation. Thus, single-crystal X-ray analysis reveals that α-CD and $KAu(CN)_2$ form a 1:1 adduct (Figures 11a and 11b) under slow evaporation conditions and a 2:1 adduct by slow diffusion of EtOH into an aqueous solution. In both cases, adduct formation in the solid state is sustained by multiple [C–H···π] and [C–H···anion] interactions between cyanide ligands in the first coordination sphere and α-CD in the second sphere. The K^+ counterions link the α-CD tori in the crystal by forming (Figure 11c) coordinative [K^+···O] bonds with glucose residues.

In aqueous solution, the existence of the 1:1 adduct between $KAu(CN)_2$ and α-CD was demonstrated by ^1H NMR titration and isothermal titration calorimetry. The binding affinity was determined to be on the order of 10^4 M^{-1}. Adduct formation in an aqueous solution is driven by a favorable enthalpy change that overcomes a minor entropic penalty. This 1:1 adduct formation between $KAu(CN)_2$ and α-CD in aqueous solution is highly selective. When β- or γ-CD are used, the binding affinities dropped to around 10^2 and 10^1 M^{-1}, respectively. Although $KAg(CN)_2$ was also found to form a 1:1 adduct with α-CD in aqueous solution, the binding affinity is an order of magnitude lower than that of $KAu(CN)_2$. This property of second-sphere coordination can be applied (Figure 11d) to the stripping of gold from the surface of activated carbon into aqueous solution at room temperature. Moreover, the stripping process is selective for $Au(CN)_2^-$ in the presence of $Ag(CN)_2^-$, making this new

DOI: 10.31635/ccschem.021.202101286
Corrected Citation: *CCS Chem.* **2022**, 4, 755–784
Previous Citation: *CCS Chem.* **2021**, 3, 3436–3465
Link to VoR: https://doi.org/10.31635/ccschem.021.202101286

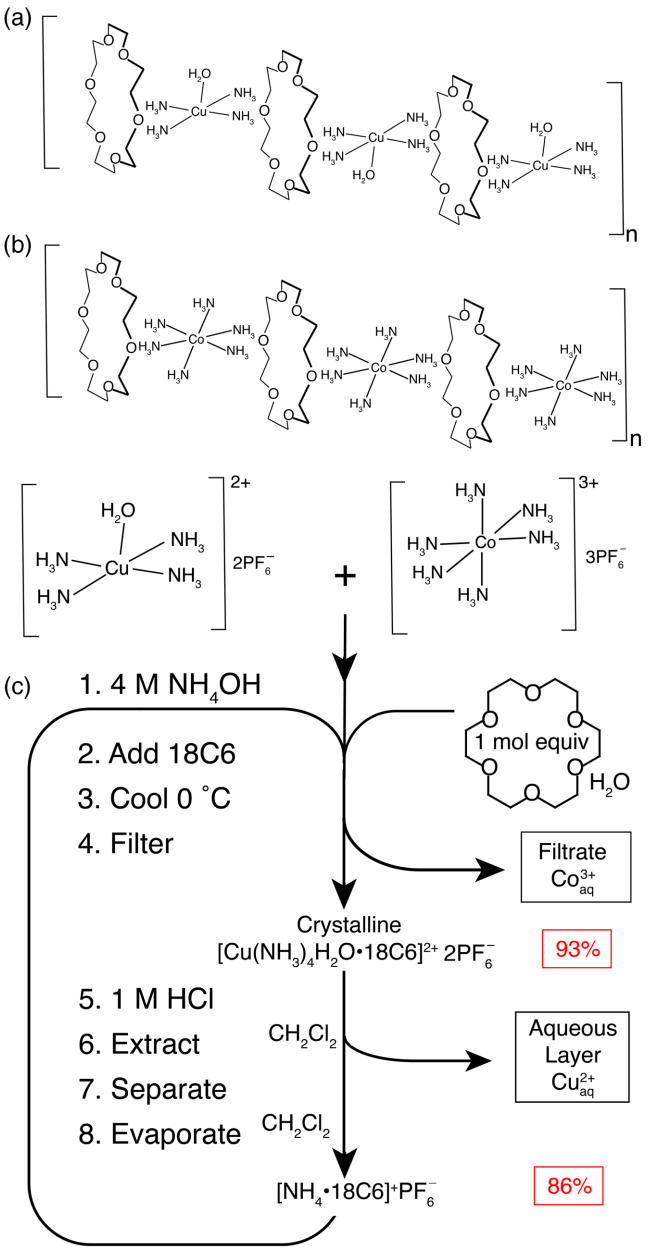

Figure 9 | *A cyclic process for the separation of Cu^{2+} from Co^{3+} based on second-sphere coordination. When one molar equivalent of 18C6 was added to a solution containing one molar equivalent each of $[Co(NH_3)_6][PF_6]_3$ and $[Cu(NH_3)_4(H_2O)][PF_6]_2$, the 1:1 copper adduct was precipitated exclusively in >90% yield. A simple filtration can separate the precipitated copper adducts from the cobalt-containing solution. The 18C6 ligand can be recovered by treating the 1:1 adduct with HCl solution, which yields aqueous copper(II) and insoluble $[NH_4][PF_6]$•18C6. The ammonium hexafluorophosphate adduct with 18C6 could be used again in separating $[Cu(NH_3)_4(H_2O)]^{2+}$ from $[Co(NH_3)_6]^{3+}$. Adapted with permission from ref 25. Copyright 1986 John Wiley and Sons.*

carbon-in-pulp process particularly attractive for mining gold ores with a high silver-content. In principle, molecular recognition processes could be integrated into commercial gold-mining protocols and lead to significantly reduced costs, energy consumption, and environmental impact.

We at NU have also developed[186,187] an eco-friendly gold recovery protocol based on the serendipitous discovery of adduct formation between α-CD and $KAuBr_4$. In an attempt to grow a CD-MOF[188–191] using $KAuX_4$ (X = Cl/Br), we observed instantaneous formation of a brown precipitate (Figure 12a) on adding an aqueous solution of $KAuBr_4$ to a solution of α-CD in water. The X-ray superstructure of crystals from this precipitate revealed a 1:2 second-sphere adduct between $KAuBr_4$ and α-CD (superstructure at left in Figure 12b), forming a one-dimensional polymeric $\{[K(OH_2)_6][AuBr_4]\subset(\alpha\text{-CD})_2\}_n$ superstructure.[186] The first-sphere ligands H_2O and Br^- are encapsulated by the second-sphere ligand α-CD. The α-CDs are packed alternately in head-to-head and tail-to-tail fashion, leading to the formation of closely packed, one-dimensional channels. The K^+ is coordinated by six H_2O ligands, forming an octahedrally coordinated $[K(OH_2)_6]^+$ ion which is sandwiched between the secondary faces of two α-CDs. This type of encapsulation is unusual considering the fact that here a fully hydrated K^+ ion is buried inside a hydrophobic binding cavity. The hydrophobic $AuBr_4^-$ ion with a square-planar coordination geometry is encapsulated between the primary faces of two α-CDs, where each primary face is occupied with a Br^- ligand. The hydrophobic effect, plus [C–H···Br–Au] hydrogen bonds between $AuBr_4^-$ and the 12 H-5 and H-6 atoms on the primary faces of α-CDs, provide the driving forces for second-sphere coordination of $AuBr_4^-$ with α-CDs. It is also worth mentioning that, inside the one-dimensional channel formed by α-CD, the two first-sphere coordination complexes line up with alternate positive and negative charges, stabilizing the overall superstructures by electrostatic interactions.

The coprecipitation process between α-CD and $KAuBr_4$ is highly selective. No precipitate is obtained when α-CD is replaced with β- or γ-CD, which do not encapsulate the $[K(OH_2)_6]^+$ counterion complex. Although these larger cyclodextrins fail to induce formation of the low-solubility superstructure with $KAuBr_4$, they do afford (Figure 12b) some more soluble complexes. Also, the use of $KAuCl_4$ does not induce coprecipitation with α, β, or γ-CD, though again, more soluble complexes can be isolated. The highly selective precipitation of $KAuBr_4$ with α-CD can even be achieved in the presence of other coordination complexes, including PtX_4^{2-} and PdX_4^{2-} (X = Cl/Br). The gold recovery efficiency is highly dependent on the counterions of $AuBr_4^-$, with the K^+ ion delivering by far the highest yield (~80%)

DOI: 10.31635/ccschem.021.202101286
Corrected Citation: *CCS Chem.* **2022**, 4, 755–784
Previous Citation: *CCS Chem.* **2021**, 3, 3436–3465
Link to VoR: https://doi.org/10.31635/ccschem.021.202101286

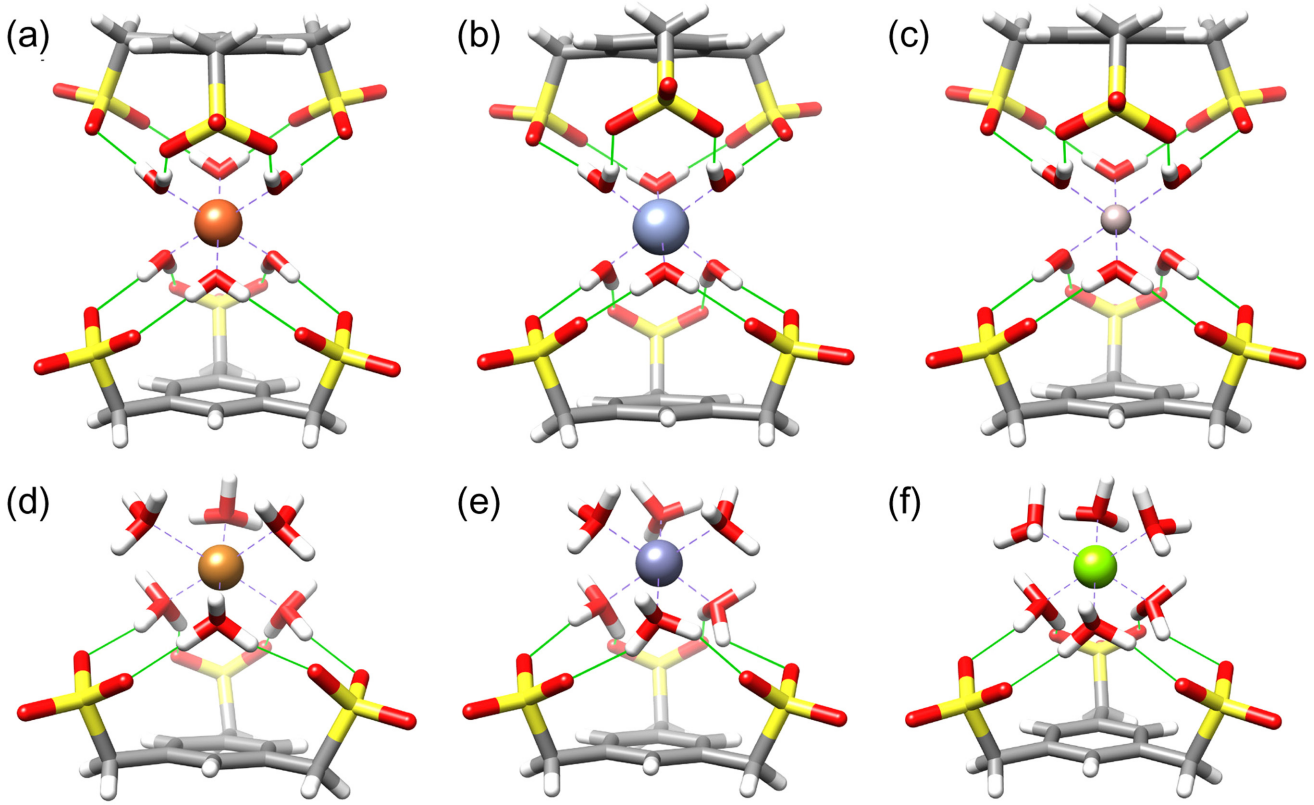

Figure 10 | *Tubular and space-filling representation of 2:1 adducts between acyclic sulfonate ligand and (a) $[Fe(OH_2)_6]^{3+}$, (b) $[Cr(OH_2)_6]^{3+}$, and (c) $[Al(OH_2)_6]^{3+}$. Tubular and space-filling representation of 1:1 adducts between acyclic sulfonate ligand and (d) $[Cu(OH_2)_6]^{2+}$, (e) $[Zn(OH_2)_6]^{2+}$, and (f) $[Mg(OH_2)_6]^{2+}$. A competitive crystallization can be employed to separate $Fe^{3+}$from Zn^{2+}. Equimolar amounts of the acyclic sulfonate ligand, $Fe(NO_3)_3$, and $Zn(NO_3)_2$ were combined in an aqueous solution. Diffusion of methanol into this mixture afforded only yellow crystals of the 1:1 adduct between the ligand and Fe^{3+} aqua complex, leaving all the Zn^{2+} in solution.*

of precipitated complex. Gold recovery decreases to 0%, 41%, and 61% for Na^+, Rb^+, and Cs^+, respectively.[187] Hydrated counterions are not found in the crystal structures of these latter complexes, the alkali metal ions being instead coordinated by oxygen atoms of the cyclodextrin's glucose residues. Temperature also plays an important role in the recovery yield, with lower temperatures leading to decreased solubility of the adducts: the gold recovery yield reaches 94% when the coprecipitation is carried out at 0 °C.

A laboratory-scale gold-recovery process has been developed (Figure 13) based on this highly selective, simple, fast, and efficient coprecipitation method. Two scrap gold-bearing alloys containing 58 wt % of Au and 42 wt % of other metals (Zn, Cu, and Ag) were converted into $HAuBr_4$ by dissolving them in a mixture of the concentrated acids HBr and HNO_3 and then neutralizing the solutions with aqueous KOH. When α-CD was added to both solutions, coprecipitation occurred immediately in the presence of other metal ions, including Zn^{2+} and Cu^{2+}. The coprecipitated adduct—containing the recovered gold—was separated by filtration and then treated with a reductant, specifically $Na_2S_2O_5$, to afford the recovered metal. The gold recovery from the two samples of gold scrap resulted in 89% yield with 97% purity and 92% yield with 95% purity.[186] For a larger, industrial-scale gold-recovery process, $KAuBr_4$ can be generated in situ using an etchant solution that is either composed of KBr, Br_2, and H_2O (Figure 13a) or KBr, O_3, and H_2O_2 (Figure 13b). This gold recovery process is much more environmentally benign in comparison with the universally accepted cyanide process. In view of the economic feasibility of the process, a startup company, Cycladex, was established in 2014. The Cycladex process has several advantages over the cyanide protocol, including faster leaching times, higher gold recovery efficiency, reduced environmental concerns, lower cost, and lower capital expenditure. The Tao group[192,193] and our own NU-based team[194] discovered, simultaneously and independently, that cucurbit[*n*]urils (CB[*n*], *n* = 5–8) are superior second-sphere ligands for AuX_4^- (X = Cl/Br) and lead[194] to instant coprecipitation (Figure 14a) of the adduct from aqueous solution. Instead

DOI: 10.31635/ccschem.021.202101286
Corrected Citation: *CCS Chem.* **2022**, 4, 755–784
Previous Citation: *CCS Chem.* **2021**, 3, 3436–3465
Link to VoR: https://doi.org/10.31635/ccschem.021.202101286

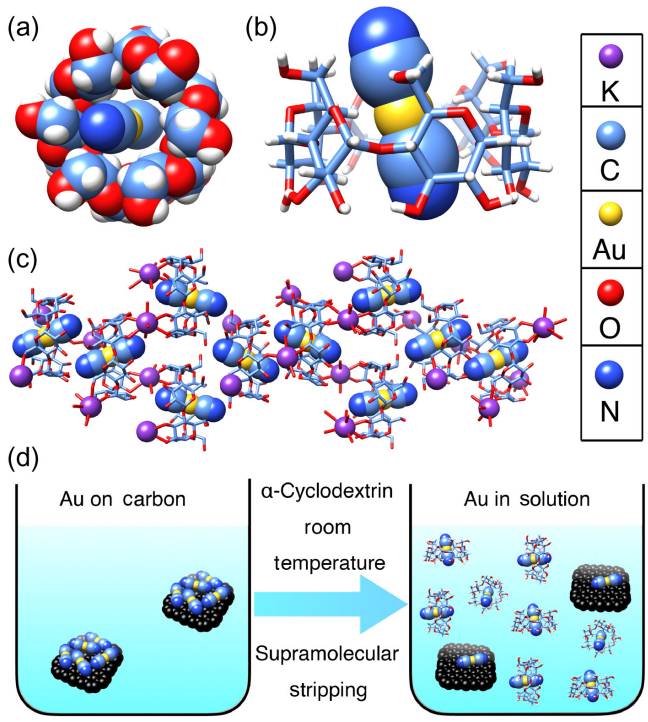

Figure 11 | *(a) Space-filling and (b) tubular representations of the X-ray superstructure of an adduct between α-CD and the $Au(CN)_2^-$ anion. (c) Stick and space-filling representation of the crystal packing between $Au(CN)_2^-$ anions and α-CDs, showing the positions of K^+ cations and $Au(CN)_2^-$ anions. (d) Graphical illustration of gold stripping from the surface of activated carbon into aqueous solution using α-CD at room-temperature. Adapted with permission from ref 185. Copyright 2021 American Chemical Society.*

of encapsulating the AuX_4^- ions inside the binding cavity, cucurbiturils interact with AuX_4^- through their outer surfaces. The X-ray superstructure of an adduct between CB[6] and $HAuCl_4$ reveals that each CB[6] is associated (Figure 14b) with four $AuCl_4^-$ ions through a combination of [Au–Cl···C=O] ion-dipole and [Au–Cl···H–C] hydrogen-bonding interactions between the Cl atoms in $AuCl_4^-$ and the methine hydrogen atoms on the outer surface of CB[6]. The solid-state superstructure of the adduct between CB[6] and $HAuBr_4$ is quite different from that of the adduct between CB[6] and $HAuCl_4$. The $AuBr_4^-$ anions exhibit two types of binding with CB[6] molecules. One of the $AuBr_4^-$ anion is connected with two CB[6] molecules located (Figure 14c) in adjacent layers, as a result of [Au–Br···H–C] interactions. The other $AuBr_4^-$ anion interacts with five CB[6] molecules through [Au–Br···H–C] hydrogen-bonding and [Au–Br···C=O] interactions.

Gold recovery using CB[6] is highly efficient: the yield is between 93% and 96% depending on the halide ligands of AuX_4^- and its counter cations. Additionally, a laboratory-scale gold-recovery protocol has been developed using a yellow gold-bearing alloy wire, which contains 58 wt % of Au and 42 wt % of Cu, Zn, and Ag. The gold portion of the alloy wire was converted to a solution of $HAuCl_4$ by dissolving it in a mixture of HCl and H_2O_2. When an aqueous solution of CB[6] is added to this gold-containing solution, coprecipitation of the adduct between CB[6] and $HAuCl_4$ occurs immediately. Elemental analysis revealed that 99.8% of the gold present in the raw material was recovered, and its purity is 98.1%. The CB[6] can be recovered by recrystallization, providing yet another opportunity to develop more efficient processes for gold recovery.

Gong et al.[195] have reported a tetracationic imidazolium cyclophane, which acts (Figure 15a) as a receptor to coprecipitate square-planar coordination complexes of noble metals—$AuCl_4^-$, $PtCl_4^{2-}$, and $PdCl_4^{2-}$—from aqueous solution. Single-crystal X-ray superstructures (Figures 15b–15d) of the adducts formed between this receptor and $AuCl_4^-$, $PtCl_4^{2-}$, and $PdCl_4^{2-}$ were obtained. Although the formation of these adducts involves [C–H···Cl–M] hydrogen-bonding, anion-π, and electrostatic interactions, the coordination complexes do not have strong directional preferences or shape selectivity for the structurally flexible cyclophane. The coprecipitation is thus driven primarily by the formation of hydrophobic ion pairs in aqueous solution.

Smith et al.[196] have developed a precise molecular recognition process (Figure 16) for the square planar ions $[AuX_4]^-$ (X = Cl/Br) using a durene-based tetralactam macrocycle. The cavity of this receptor is preorganized (Figures 16a and 16b) with four convergent hydrogen-bond donors to interact with the electronegative halide ligands. Meanwhile, the receptor possesses a pair of parallel arene units (durene residues) as π-electron donors to interact with the electropositive metal center. Several single-crystal X-ray superstructures were obtained (Figures 16c and 16d) of the adducts between this receptor and coordination complexes of precious metals, including AuX_4^- (X = Cl/Br), $PtCl_4^{2-}$, and $Pd_2Cl_6^{2-}$, which confirmed the presence of the hydrogen bonds and [metal···π] interactions. These second-sphere coordination adducts were also shown to exist in solution, with ^{1}H NMR titrations indicating that their stability in solution depends on the nature of both the halide ligands and the metals. The binding affinity of $AuCl_4^-$ (K_a = 7.8 × 10^4 M^{-1}) is about 30 times stronger than that of $AuBr_4^-$ (K_a = 2.5 × 10^3 M^{-1}). When the metal center is changed from Au(III) to Pt(II), the binding affinity (X = Cl) was decreased by a factor of 3900 to K_a = 20 M^{-1}, highlighting the critical role of [metal···π] interactions. Addition of the receptor to a solution of $HAuCl_4$ or $HAuBr_4$ in an organic solvent led to instant coprecipitation of the adducts. In subsequent work, Jiang et al.[197] have developed a similar 2,3-dibutoxynaphthalene-based tetralactam macrocycle that can capture $AuCl_4^-$ from organic solution. Molecular modeling suggests that

DOI: 10.31635/ccschem.021.202101286
Corrected Citation: *CCS Chem.* **2022**, 4, 755–784
Previous Citation: *CCS Chem.* **2021**, 3, 3436–3465
Link to VoR: https://doi.org/10.31635/ccschem.021.202101286

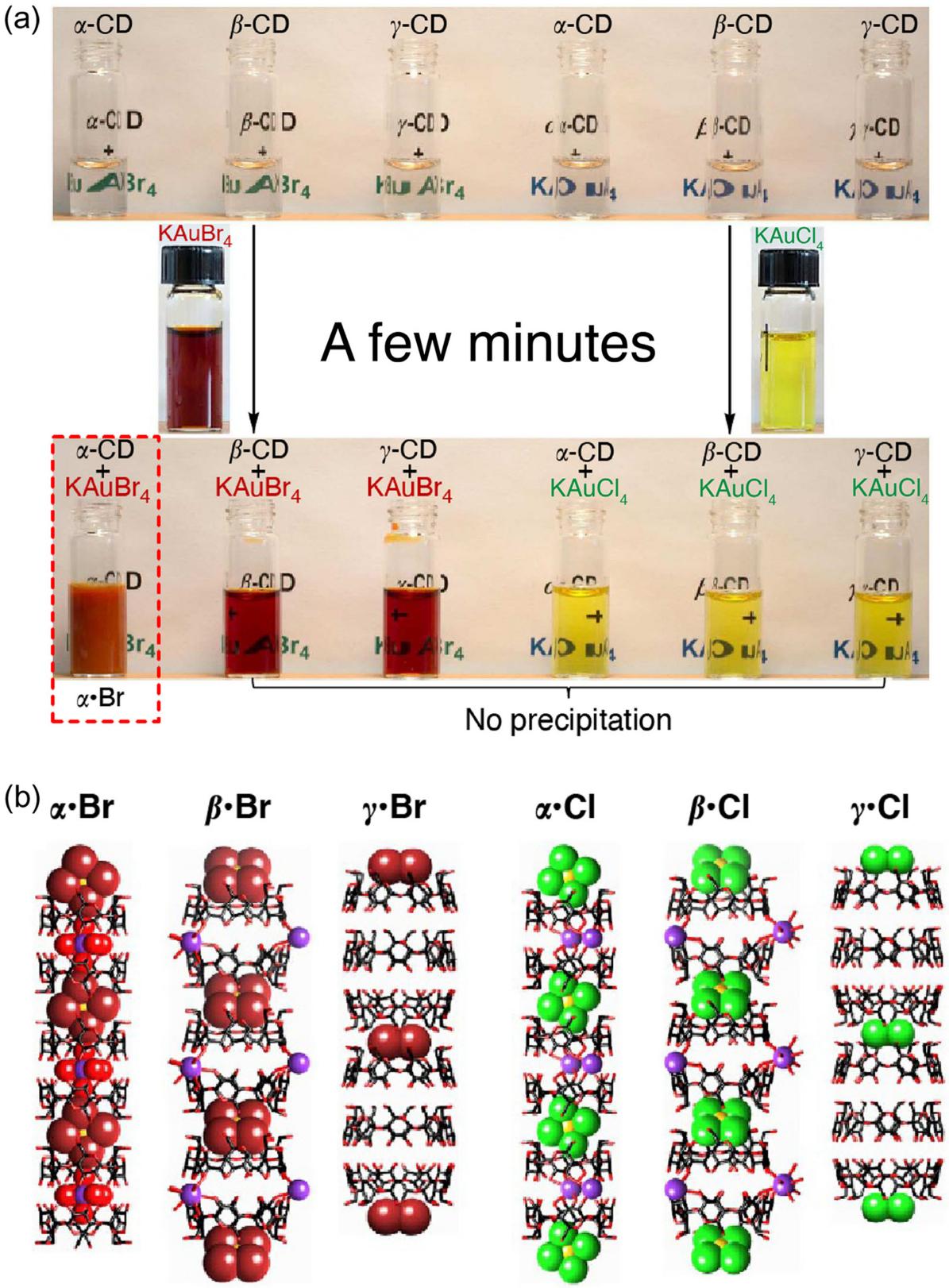

Figure 12 | *(a) Selective formation of a coprecipitate α-CD•KAuBr$_4$. The brown precipitate formed instantly when adding an aqueous solution of KAuBr$_4$ into a solution of α-CD in H$_2$O. (b) Stick and space-filling representation of the X-ray superstructures of α-CD•KAuBr$_4$, β-CD•KAuBr$_4$, γ-CD•HAuBr$_4$, α-CD•KAuCl$_4$, β-CD•KAuCl$_4$, and γ-CD•HAuCl$_4$. The major reason for the adduct co-precipitation between α-CD and KAuBr$_4$ is that they form a one-dimensional polymeric {[K(OH$_2$)$_6$][AuBr$_4$]⊂(α-CD)$_2$}$_n$ superstructure. Adapted with permission from ref 186. Copyright 2013 Springer Nature.*

DOI: 10.31635/ccschem.021.202101286
Corrected Citation: *CCS Chem.* **2022**, 4, 755–784
Previous Citation: *CCS Chem.* **2021**, 3, 3436–3465
Link to VoR: https://doi.org/10.31635/ccschem.021.202101286

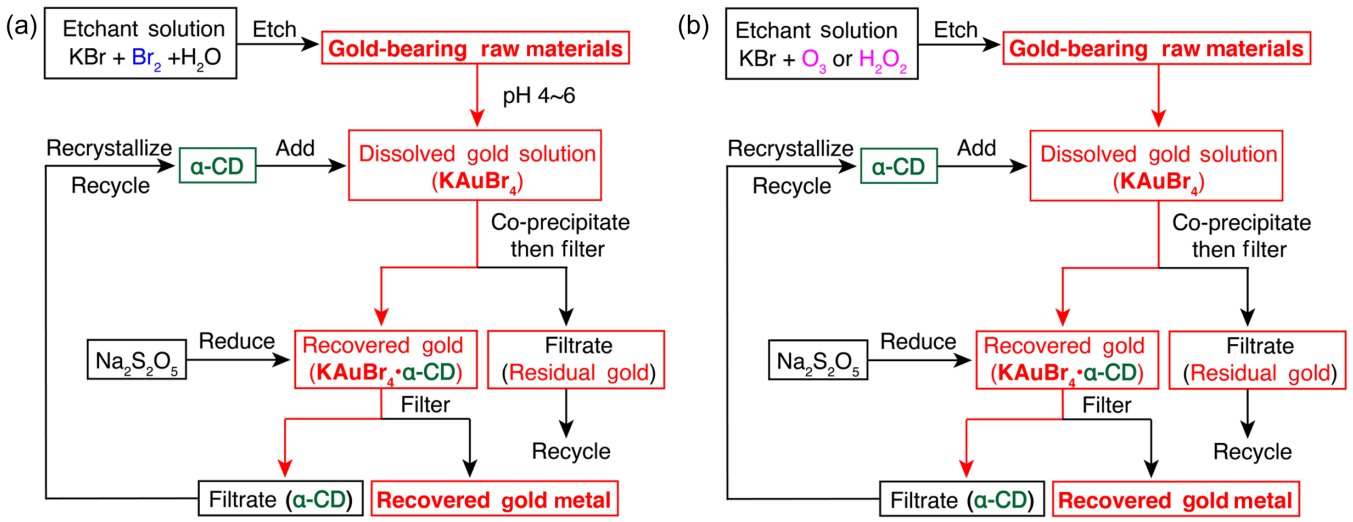

Figure 13 | *Flow diagrams of gold recovery based on the formation of the insoluble 1:1 adduct between α-CD and $[K(OH_2)_6]^+[AuBr_4]^-$. $KAuBr_4$ can be generated in situ using an etchant solution that is either composed of (a) KBr, Br_2, and H_2O or a greener oxidant (b) KBr, O_3, and H_2O_2. Red arrows indicate the flow direction of the gold recovery. $Na_2S_2O_5$ = Sodium metabisulfite.*

adduct formation is sustained by the same patterns of noncovalent bonding interactions.

In an effort to direct the molecular recognition process toward a practical gold-recovery technology, Smith et al.[198] have developed (Figures 16e and 16f) an acyclic system that can be made to work in a similar manner to their tetralactam macrocycle[196] for the coprecipitation of gold halides. The acyclic amides can be rendered soluble in either organic or aqueous solvents, depending on the constitution of the solubilizing R groups. These acyclic receptors and the gold(III) halide complexes coprecipitate instantly from solution. X-ray diffraction analysis of the recrystallized coprecipitates reveals (Figures 16g and 16h) a similar pattern of noncovalent-bonding interactions to the binding of the gold halides by the tetralactam macrocycle involving an array of hydrogen bonds in addition to [Au···π] interactions. These acyclic receptors with low molecular weights can be prepared cheaply on a large scale, rendering them attractive molecules for the development of next-generation gold-recovery technologies.

Catalysis

Natural enzymes perform catalytic reactions at lightning speeds and with high substrate selectivities using a potent catalytic center within a nanoconfined pocket[91,199] constructed by chain-folding of a protein molecule. The superstructure of an enzyme-binding pocket not only dictates the substrate selectivity but also isolates the catalytic center from other reactive sites. This compartmentalization of different catalytic centers enhances[200] the stability of a given catalytic center and extends its functional lifetime. Following pioneering research by Breslow et al.[201-208] in the 1970s using cyclodextrins and their derivatives, there have been continued efforts to develop enzyme analogues that allow catalytic reactions to be performed in confined nanoenvironments.[91,199] Significant advances have been made in creating these artificial enzymes, as summarized[209-219] in several excellent reviews. It turns out that second-sphere coordination has been exploited widely as an emerging strategy for designing artificial enzymes by encapsulating catalysts inside molecular containers, leading to high efficiencies and excellent regio- and stereoselectivities being achieved at the catalytic centers.

Sollogoub et al. [220] have demonstrated a good example of regioselectivity that involves switching using covalent *N*-heterocyclic carbene-capped α- and β-cyclodextrins as second-sphere coordination ligands, encapsulating a Cu(I)Cl catalyst. The resulting catalysts, α- and β-CD-CuCl, were investigated (Figure 17a) for copper-catalyzed hydroboration of substituted and unsubstituted terminal and internal phenylalkynes. It was found that α-CD-CuCl results in excellent selectivity for the linear products (Figure 17b), yielding a branched-to-linear (B/L) ratio of 9:91. By contrast, the β-CD-CuCl catalyst leads mainly to branched products, with a B/L ratio of 90:10. The changed shape of the cavity promotes, not only a regioselectivity switch, but also a mechanistic switch. Density functional theory (DFT) calculations indicate that the cavity of α-CD-CuCl promotes an orthogonal approach of acetylene, leading to a linear product. The larger cavity of β-CD-CuCl favors instead a parallel approach, in which the alkyne projects directly into the cavity.

In a subsequent investigation, the same authors reported[221] another example (Figure 17c) of

DOI: 10.31635/ccschem.021.202101286
Corrected Citation: *CCS Chem.* **2022**, 4, 755–784
Previous Citation: *CCS Chem.* **2021**, 3, 3436–3465
Link to VoR: https://doi.org/10.31635/ccschem.021.202101286

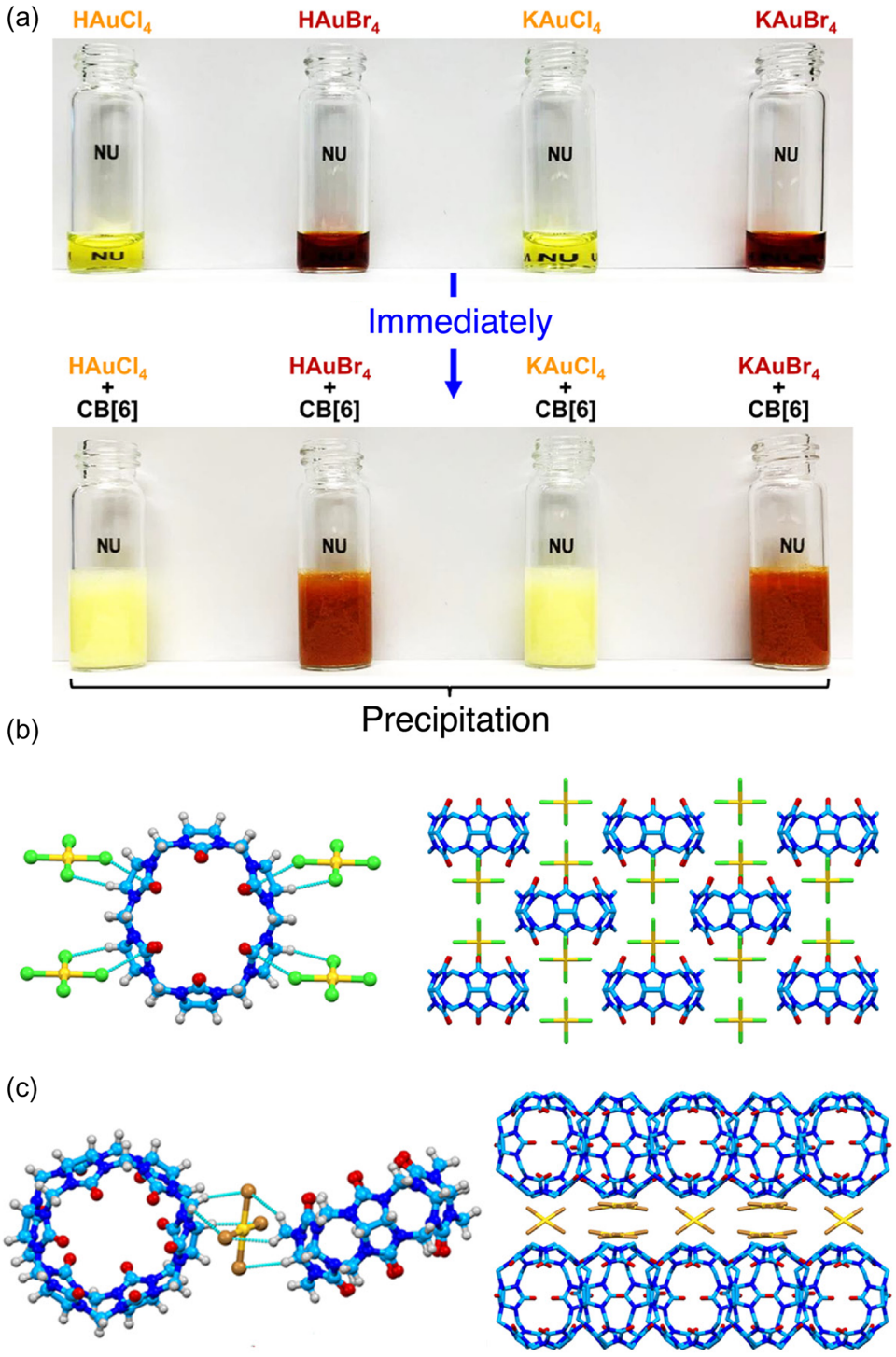

Figure 14 | *(a) Rapid formation of coprecipitates CB[6]•MAuX$_4$ (M = H/K, X = Cl/Br) from a mixture of CB[6] and MAuX$_4$ in aqueous solution. (b) Ball-and-stick representation of X-ray superstructure of the adduct between CB[6] and AuCl$_4^-$. Each CB[6] is associated with four AuCl$_4^-$ anions through a combination of [Au–Cl···C=O] ion-dipole interactions and [Au–Cl···H–C] hydrogen-bonding interactions between the Cl atoms in AuCl$_4^-$ and the methine hydrogen atoms on the outer surface of CB[6]. (c) Ball-and-stick representation of X-ray superstructure of the adduct between CB[6] and AuBr$_4^-$. The AuBr$_4^-$ anions exhibit two types of binding with CB[6] molecules. One of the AuBr$_4^-$ anion is associated with two CB[6] molecules located in adjacent layers as a result of [Au–Br···H–C] interactions. The other AuBr$_4^-$ anion interacts with five CB[6] molecules through the [Au–Br···H–C] hydrogen-bonding and [Au–Br···C=O] interactions. Adapted with permission from ref 194. Copyright 2020 American Chemical Society.*

DOI: 10.31635/ccschem.021.202101286
Corrected Citation: *CCS Chem.* **2022**, 4, 755–784
Previous Citation: *CCS Chem.* **2021**, 3, 3436–3465
Link to VoR: https://doi.org/10.31635/ccschem.021.202101286

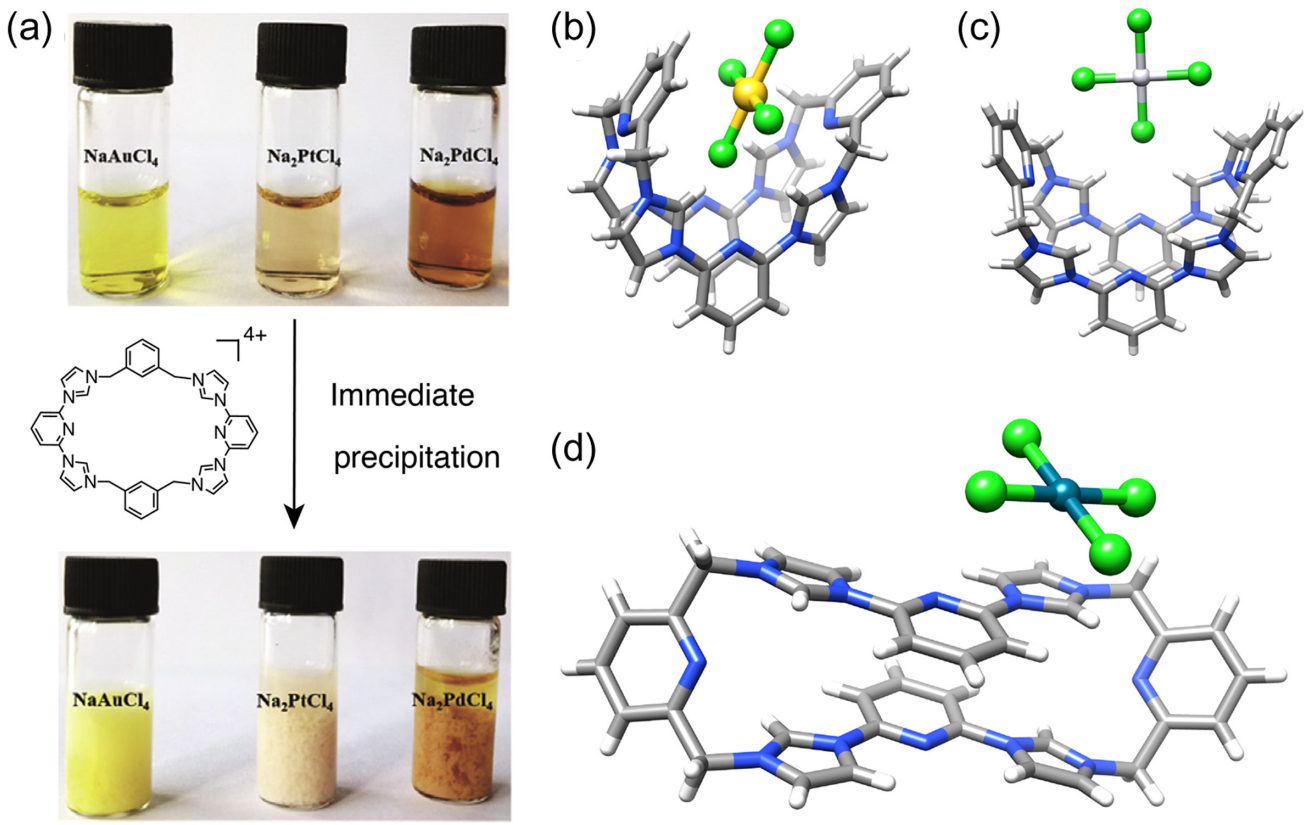

Figure 15 | *(a) Rapid formation of coprecipitates cyclophane•MX_4^{n-} (M = Au/Pt/Pd, n = 1 or 2) in aqueous solution. Ball-and-stick representations of X-ray superstructures between cyclophane and (b) $AuCl_4^-$, (c) $PtCl_4^{2-}$, and (d) $PdCl_4^{2-}$. These noble-metal coordination complexes do not have strong directional preference or shape selectivity for the structurally flexible cyclophane. The coprecipitation is driven primarily by the formation of hydrophobic ion pairs in an aqueous solution. Adapted with permission from ref 195. Copyright 2018 Elsevier.*

regioselective catalysis using these two cyclodextrin-based catalysts for the hydrosilylation of α,β-unsaturated enones. The very reactive monomeric hydride (L)CuH is stabilized inside the cavity, leading to the high efficiencies exhibited by these two catalysts. Remarkably, exclusive 1,2-addition is observed using α-CD-CuCl, with good enantiomeric excesses. In contrast, the β-CD-CuCl catalyst, with its larger binding cavity, promotes the full reduction of the substrate. The difference in selectivity for these two catalysts can be attributed to the difference in the sizes of the binding cavities, which control the accessibility of the substrate to the catalytic Cu(I) center. Additionally, the interactions between CDs and their substrates favor 1,2-addition for α-CD-CuCl and 1,4-addition for β-CD-CuCl. This example demonstrates the ability of the two cyclodextrin-based ligands to stabilize the reactive catalytic center and select for different orientations of the substrate, resulting in highly effective catalysis with excellent regioselectivities.

The Raymond, Bergman, and Toste triumvirate[211,216,222–224] at UC Berkeley have investigated numerous catalysts within confined nanospaces by exploiting a family of polyanionic tetrahedral cages that function as second-sphere ligands for the encapsulation of catalysts composed of coordination complexes. For example, they have reported (Figure 18a) a rare example of site-selective hydrogenation of alkenes, promoted[223] by a catalyst composed of a naphthalene-based gallium(III) cage ("Naph-Cage") encapsulating a cationic (DMPE)Rh(COD) precursor (DMPE = 1,2-bis(dimethylphosphino)ethane; COD = 1,5-cyclooctadiene). Using this cage-encapsulated catalyst, the authors observed high conversions of alkenes where the double bond is remote from the hydroxyl group, as in 5- and 4-hexen-1-ols. Conversely, little or no conversion of the double bonds more proximate to the hydroxy groups presented in 3- and 2-hexen-1-ols was observed under the same conditions. Moreover, the free Rh catalyst operating in bulk solution led to a quantitative conversion of all hexen-1-ol substrates, regardless of the position of the C=C double bond. The site-selectivity of this cage-encapsulated catalyst has been attributed to preferential binding of the more lipophilic alkyl end of the pendant alcohol substrate within the cavity. In a further demonstration of site-selective hydrogenation, the authors showed[223] that the fatty alcohol of lineolenic acid (Figure 18b), which contains three points of unsaturation, undergoes only

DOI: 10.31635/ccschem.021.202101286
Corrected Citation: *CCS Chem.* **2022**, 4, 755–784
Previous Citation: *CCS Chem.* **2021**, 3, 3436–3465
Link to VoR: https://doi.org/10.31635/ccschem.021.202101286

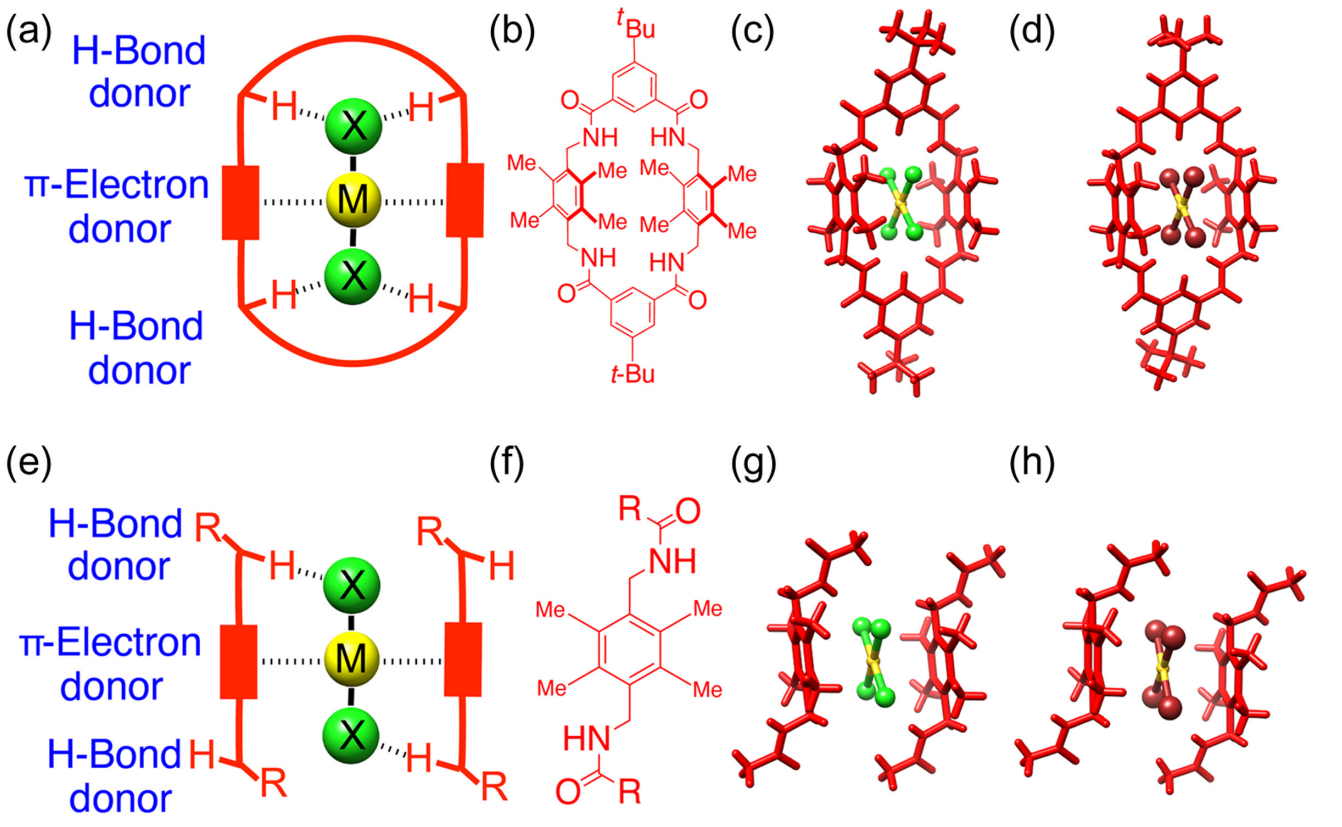

Figure 16 | *(a) Schematic illustration of binding AuX_4^- with cyclophane through two sets of directional interactions, that is, hydrogen bonding and Au-aromatic stacking. (b) The structural formula of a durene-based tetralactam macrocycle. Ball-and-stick representations of the X-ray solid-state superstructure of the adducts of macrocycle with (c) $AuCl_4^-$ and (d) $AuBr_4^-$. (e) Schematic illustration of binding AuX_4^- with acyclic ligands through two sets of directional interactions (hydrogen bonding and Au-aromatic stacking). (f) The structural formula of a durene-based acyclic ligand. Ball-and-stick representations of the X-ray solid-state superstructure of the adducts of a durene-based acyclic ligand with (g) $AuCl_4^-$ and (h) $AuBr_4^-$. Adapted with permission from ref 196. Copyright 2018 American Chemical Society.*

monohydrogenation (74% yield) of the terminal double bond in the presence of a larger pyrene-based cage ("Pyr-Cage"). This example shows that supramolecular catalyst-directed regioselectivity, based on second-sphere coordination, can overcome any inherent selectivity deriving from the substrate or a nonencapsulated catalyst.

Second-sphere coordination of transition-metal catalysts has also been shown to enhance enantioselective transformations. Reek et al.[225] have reported the encapsulation of a chiral Rh complex in an achiral supramolecular cage (Figure 19a) formed by coordination-driven self-assembly of a macrocyclic dipalladium complex and a tetracarboxylate zinc porphyrin. The resulting encapsulated catalyst is highly active in the case of the hydroformylation of styrene and derivatives (Figure 19b), which were converted into aldehydes with a much higher chiral induction—up to 71% e.e.—than with the free Rh catalyst. The stereoselectivity demonstrated by the encapsulated catalyst is based on controlling the second-sphere coordination by way of the structural constraints imposed by the cage. The same group has also described several examples in which second-sphere coordination is able to control regioselectivity in hydroformylation reactions.[226–230]

MOFs can be synthesized with a wide range of nodes and linkers,[2–16] making them an attractive platform for systematic engineering of second-sphere interactions. Inspired by the effectiveness of biological catalytic conversion of carbon dioxide to the glucose precursor glyceraldehyde-3-phosphate, performed in compartmentalized organelles, Tsung et al.[231] have investigated (Figure 20) the influence of second-sphere coordination on catalytic reactivity in the hydrogenation of carbon dioxide to methanol, using MOF UiO-66 as the second-sphere ligand to encapsulate a transition-metal catalyst. This catalytic system is composed of three components: (1) a ruthenium PNP pincer complex (green) to carry out the hydrogenation of carbon dioxide to formic acid, (2) the $Zr_6(OH)_4O_4$ metal nodes of the MOF to convert formic acid to formate ester, and (3) a second ruthenium

DOI: 10.31635/ccschem.021.202101286
Corrected Citation: *CCS Chem.* **2022**, 4, 755–784
Previous Citation: *CCS Chem.* **2021**, 3, 3436–3465
Link to VoR: https://doi.org/10.31635/ccschem.021.202101286

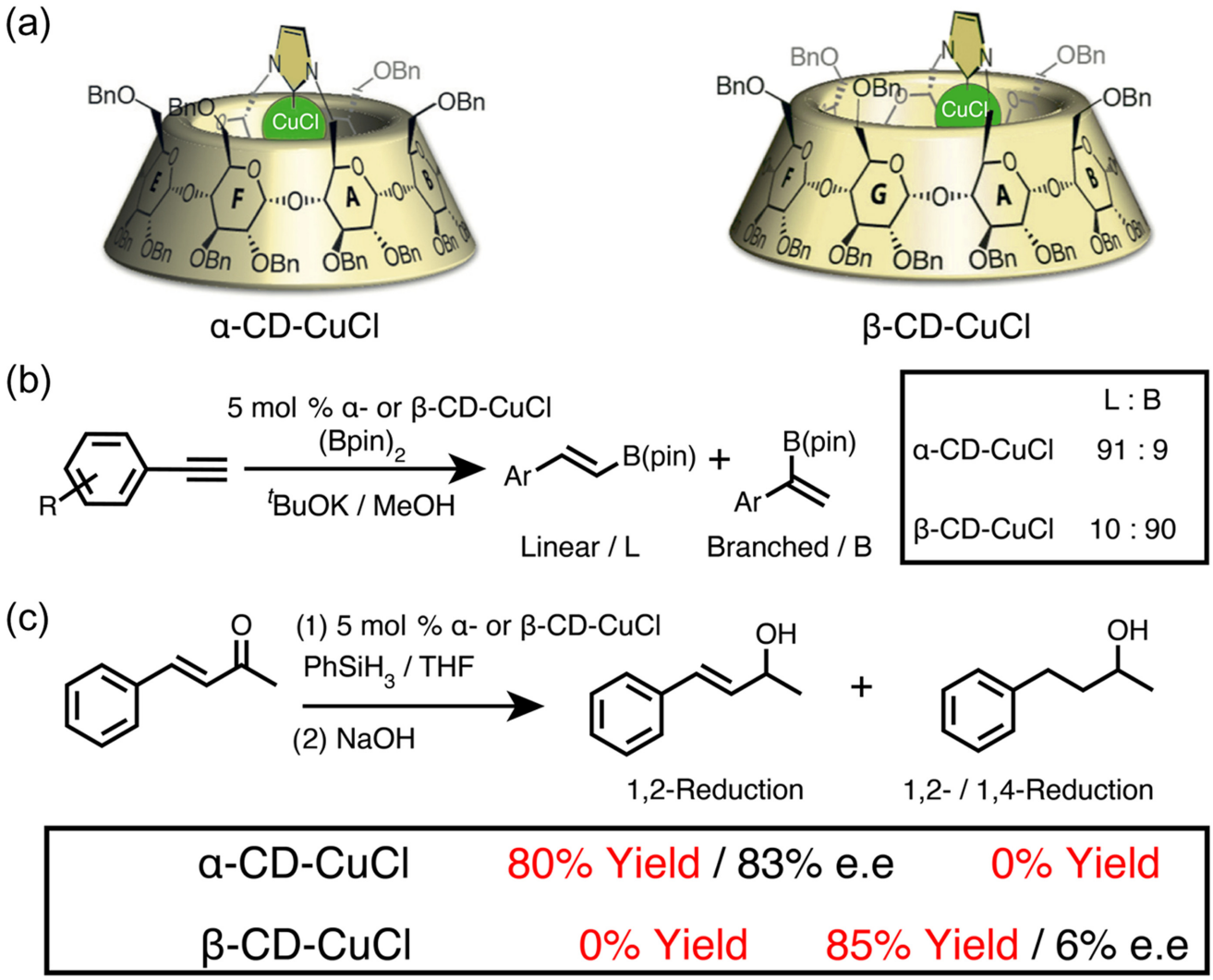

Figure 17 | *(a) Covalent N-heterocyclic carbene-capped α- and β-CDs as second-sphere coordination ligands, which encapsulate a Cu(I)Cl catalyst. (b) Copper-catalyzed hydroboration with substituted and unsubstituted terminal and internal phenylalkynes using α- and β-CD-CuCl. The use of α-CD-CuCl results in excellent selectivity for the linear products, yielding a B/L ratio of 9:91. In contrast, the β-CD-CuCl catalyst leads to the branched products with a B/L ratio of 90:10. (c) Hydrosilylation of α,β-unsaturated enones catalyzed by α- and β-CD-CuCl. Exclusive 1,2-addition using α-CD-CuCl with good enantiomeric excesses was observed. The β-CD-CuCl catalyst was found to promote the full reduction of the substrate. Adapted with permission from ref 220. Copyright 2017 John Wiley and Sons.*

PNN pincer complex (orange) to catalyze hydrogenation of the formate ester to methanol. The final product, methanol, was only observed in these cascade hydrogenation reactions when the two ruthenium complexes were separated from each other by encapsulating the PNP catalyst into the cavity of the MOF, illustrating the importance of component separation for efficient catalysis. The beneficial effects of the second-sphere coordination were investigated extensively for the first catalyst in this cascade process. The synthetic flexibility of the MOF UiO-66 allowed the authors to modify the linkers with different substituents, leading to a series of functionalized MOF UiO-66. They found that when a primary ammonium functional group, $[Ar\text{-}NH_3]^+$, is employed, the resulting UiO-66-NH_3^+ significantly improves the catalytic efficiency for hydrogenation of carbon dioxide to formic acid. Mechanistic investigations revealed that the arylammonium group functions as a general Brønsted acid. Consequently, the resulting catalyst system provides access to high catalytic performance by manipulating second-sphere interactions. The authors obtained the highest reported turnover number (TON) (19,000) and turnover frequency (TOF) (9100 h^{-1}) for hydrogenation of carbon dioxide to

DOI: 10.31635/ccschem.021.202101286
Corrected Citation: *CCS Chem.* **2022**, 4, 755–784
Previous Citation: *CCS Chem.* **2021**, 3, 3436–3465
Link to VoR: https://doi.org/10.31635/ccschem.021.202101286

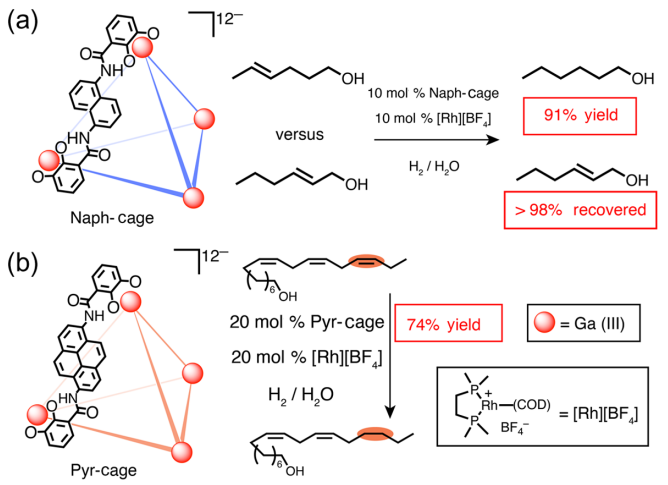

Figure 18 | *(a) The structural formula of a Naph-Cage, which can encapsulate the Rh catalyst, (DMPE)Rh(COD), for the site-selective hydrogenation of olefins. High conversions of olefins in which the double bond is remote from the hydroxyl group (5- and 4-hexen-1-ol) are seen. Meanwhile, little or no conversion of more proximate double-bonds (3- and 2-hexen-1-ol) was observed under the same catalytic conditions. (b) The structural formula of a Pyr-Cage which encapsulates a Rh catalyst, catalyzing mono-hydrogenation of the fatty alcohol of lineolenic acid that contains three points of unsaturation. Adapted with permission from ref 223. Copyright 2019 American Chemical Society.*

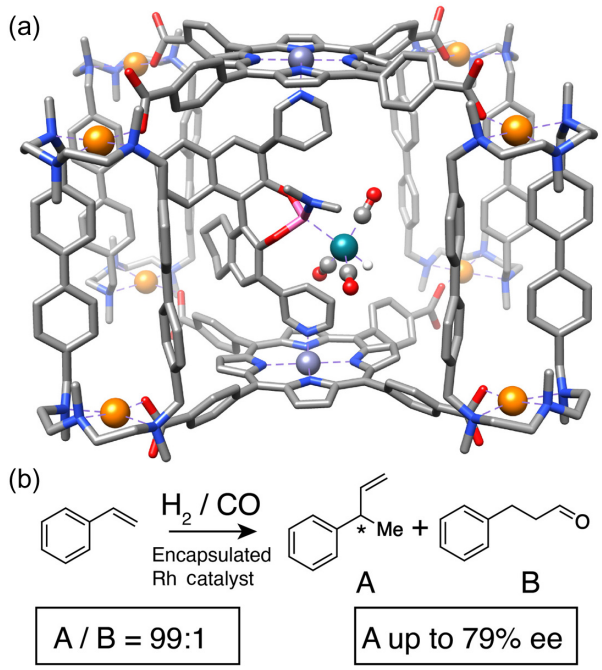

Figure 19 | *(a) Ball-and-stick representation of a chiral Rh complex in an achiral supramolecular cage formed from coordination-driven self-assembly of macrocyclic dipalladium complex and tetracarboxylate zinc porphyrins. (b) Hydroformylation of styrene and derivatives, which were converted into formyl products with a very high chiral induction of up to 71% e.e. catalyzed by the encapsulated Rh catalyst, significantly outperforming the free Rh catalyst.*

methanol. Furthermore, the recyclable nature of this system allowed the authors to achieve a cumulative TON of 100,000 after 10 reaction cycles.

Biomolecular Chemistry

Biological macromolecules have long been known to bind to transition-metal complexes, most notably, perhaps, the metal-based anticancer drugs cisplatin,[25,52] [*cis*-($Pt(NH_3)_2(Cl)_2$)], and carboplatin[53,54] that complex with DNA and inhibit its replication and transcription. These drugs react with the guanine bases of DNA in the major groove, initially via aquation, with loss of halide or carboxylate ligands, followed by direct (first-sphere) coordination of the metal center by guanine nitrogen atoms that displace the coordinated water. Over the past decade, however, it has also been established that kinetically *inert* complexes of ruthenium(II) with heterocyclic ligands such as 2,2′-bipyridine (bipy), phenanthroline (phen), and dipyridophenazine (dppz) are able to bind to double-helical DNA by a *second-sphere* mechanism (Figure 21), involving intercalation of a heterocyclic ligand between successive pairs of nucleobases, without a great deal of base specificity.[232]

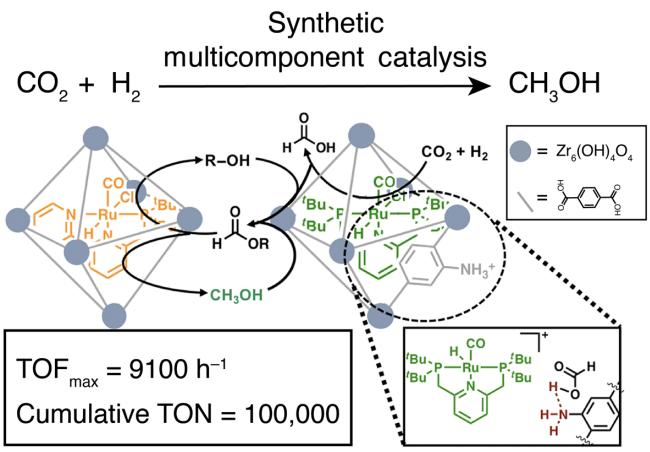

Figure 20 | *A host–guest multicomponent catalyst system for the hydrogenation of carbon dioxide to MeOH engineered by second-sphere coordination. In this system, the green ruthenium complex 1@UiO-66-NH_3^+ carries out the hydrogenation of CO_2 to HCO_2H, the blue $Zr_6(OH)_4O_4$ nodes of the MOF converts formic acid to formate ester, and the orange 2@UiO-66 carries out the hydrogenation of formate ester to MeOH. Adapted with permission from ref 231. Copyright 2021 American Chemical Society.*

DOI: 10.31635/ccschem.021.202101286
Corrected Citation: *CCS Chem.* **2022**, 4, 755–784
Previous Citation: *CCS Chem.* **2021**, 3, 3436–3465
Link to VoR: https://doi.org/10.31635/ccschem.021.202101286

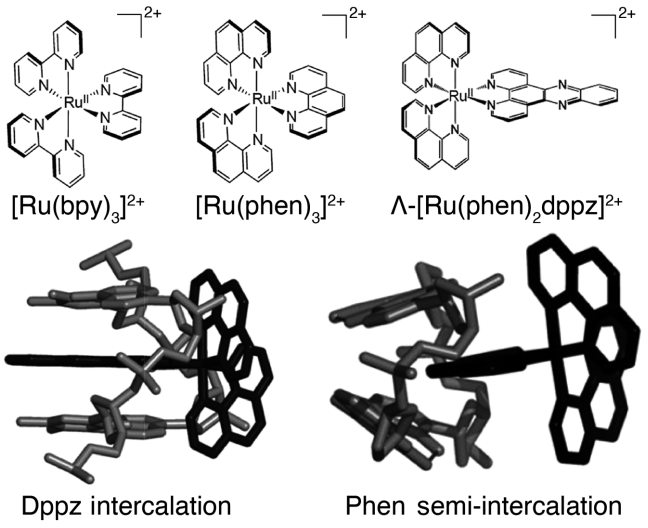

Figure 21 | *Representative DNA-binding complexes $[Ru(LL)_3]^{2+}$, with illustrative modes of intercalation into DNA between nucleobase pairs. L = Phen, bpy.*

Single-crystal X-ray studies of such systems, using double-stranded DNA oligomers (typically decamers or dodecamers), have revealed a wide range of binding geometries (Figure 22), depending to some extent on the base pairs involved but mainly on the detailed structure and chirality of the metal complex.[233–235] Given the opposite charges of the DNA host (strongly anionic) and the metal complex guest (di-cationic), together with the relatively low polarity of the heterocyclic ligands and the coplanarity of the base pairs, it seems likely that electrostatic forces, hydrophobic effects, and [π···π] stacking interactions all play significant roles in the second-sphere binding of these complexes to DNA.

Ruthenium complexes of the type shown in Figure 21 are known sensitizers for photooxidation of DNA. This observation can be turned to advantage in photodynamic cancer therapy where only targeted tissue is destroyed. Recent studies of single crystals of a DNA oligomer bound to such a photosensitizing ruthenium complex, using both X-ray crystallography and ultrafast (picosecond) infrared (IR) laser spectroscopy, have shown[236] for the first time how light absorption by the metal complex and consequent electron transfer from the readily oxidized guanine base are related to DNA damage. Such damage represents the first step in killing a tumor cell. Guanine residues are also important in the specialized drug target known as the G-quadruplex, which has a large planar aromatic surface and which correspondingly has a strong affinity for large aromatic ligands. This type of unit is particularly easy to oxidize and so there is much scope for donor–acceptor matching in the design of new therapeutic agents.[236]

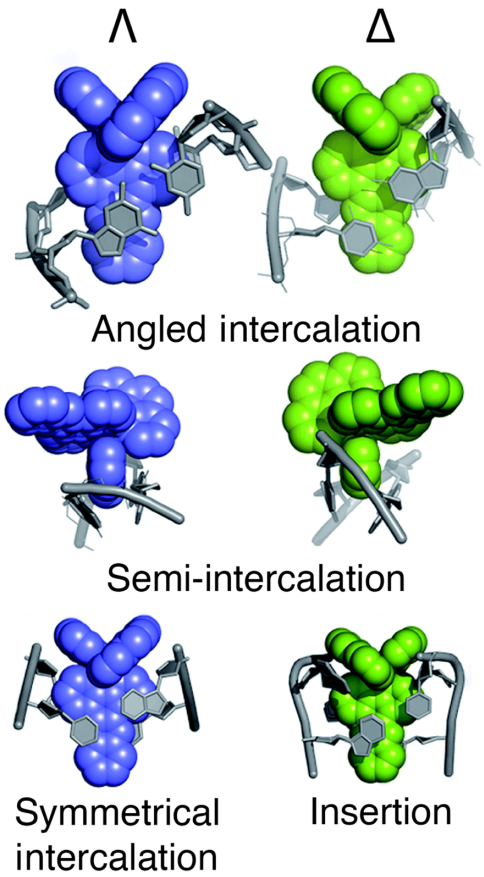

Figure 22 | *Summary of the main binding modes of the two enantiomers of $[Ru(L)_2dppz)]^{2+}$ with duplex DNA (L = phenanthroline or tetraazaphenanthroline, TAP). Λ form is shown in blue and Δ form in green. The specific binding mode adopted is dependent on the DNA sequences involved, so that the symmetrical intercalation mode, for example, has so far been found only at the duplex sequence TA/TA. This sequence specificity arises from π–π stacking of phenanthroline with the adenosine (A) residues.*

Summary and Outlook

Second-sphere coordination has emerged as a strategy to access many functional systems in molecular recognition, construction of MIMs, metal separations, catalysis, and biomolecular chemistry. The noncovalent bonding interactions between the second-sphere ligands and coordination complexes can fine-tune the chemical, physical, electrochemical, and photochemical properties of the resulting adducts, leading to numerous opportunities in creating new technologies.

As one of the future directions for this chemistry, second-sphere coordination can be employed to develop new protocols for the sustainable separation of metals. Currently, most of the effort has been focused on new strategies for gold separation by second-sphere coordination, but similar principles can undoubtedly be applied

DOI: 10.31635/ccschem.021.202101286
Corrected Citation: *CCS Chem.* **2022**, 4, 755–784
Previous Citation: *CCS Chem.* **2021**, 3, 3436–3465
Link to VoR: https://doi.org/10.31635/ccschem.021.202101286

to the separation of other metals. Second-sphere coordination can facilitate the crystallization, precipitation, leaching, and chromatographic separation in metal-purification processes, leading to selective, efficient, and green separation technologies for metals.

In the solid state, MOFs have provided a versatile platform for the operation of AMMs by harnessing the concept of second-sphere coordination. Some elegant examples of mechanically interlocked MOFs with machine-like dynamics have been demonstrated.[237–241] The operation of these molecular machines in the solid state may well provide an important route for the realization of advanced technologies in gas storage, drug delivery, and molecular separations.

Looking to the longer term, the marriage between supramolecular and coordination chemistry can clearly generate new pathways for tackling societal challenges in health, energy, and the environment. We envision that this field will attract more and more attention from multidisciplinary researchers, who will unleash the potential of this concept to advance chemistry, medicine, materials, and environmental science.

Conflicts of Interest

The authors declare no conflict of interest.

Acknowledgments

The authors thank Dr. Margaret Schott for assistance with editing and proofing of the manuscript. The authors thank Northwestern University (NU) for their support of this work, which was also funded by the Center for Sustainable Separation of Metals (CSSM) and part of a National Science Foundation (NSF) Center for Chemical Innovation (CCI): grant number CHE1925708.

References

1. Lawrance, G. A. *Introduction to Coordination Chemistry*; Wiley: Chichester, **2013**.
2. Yaghi, O. M.; Li, G.; Li, H. Selective Binding and Removal of Guests in a Microporous Metal–Organic Framework. *Nature* **1995**, *378*, 703–706.
3. Rosi, N. L.; Eckert, J.; Eddaoudi, M.; Vodak, D. T.; Kim, J.; O'Keeffe, M.; Yaghi, O. M. Hydrogen Storage in Microporous Metal–Organic Frameworks. *Science* **2003**, *300*, 1127–1129.
4. Li, Q.; Zhang, W.; Miljanić, O. Š.; Sue, C.-H.; Zhao, Y.-L.; Liu, L.; Knobler, C. B.; Stoddart, J. F.; Yaghi, O. M. Docking in Metal–Organic Frameworks. *Science* **2009**, *325*, 855–859.
5. Kreno, L. E.; Leong, K.; Farha, O. K.; Allendorf, M.; Van Duyne, R. P.; Hupp, J. T. Metal–Organic Framework Materials as Chemical Sensors. *Chem. Rev.* **2012**, *112*, 1105–1125.
6. Furukawa, H.; Cordova, K. E.; O'Keeffe, M.; Yaghi, O. M. The Chemistry and Applications of Metal–Organic Frameworks. *Science* **2013**, *341*, 1230444.
7. Bobbitt, N. S.; Mendonca, M. L.; Howarth, A. J.; Islamoglu, T.; Hupp, J. T.; Farha, O. K.; Snurr, R. Q. Metal–Organic Frameworks for the Removal of Toxic Industrial Chemicals and Chemical Warfare Agents. *Chem. Soc. Rev.* **2017**, *46*, 3357–3385.
8. Kim, H.; Yang, S.; Rao, S. R.; Narayanan, S.; Kapustin, E. A.; Furukawa, H.; Umans, A. S.; Yaghi, O. M.; Wang, E. N. Water Harvesting from Air with Metal–Organic Frameworks Powered by Natural Sunlight. *Science* **2017**, *356*, 430–434.
9. Lazaro, I. A.; Forgan, R. S. Image-Guided Therapy Using Maghemite-MOF Nanovectors. *Chem* **2017**, *3*, 200–202.
10. Kung, C.-W.; Goswami, S.; Hod, I.; Wang, T. C.; Duan, J.; Farha, O. K.; Hupp, J. T. Charge Transport in Zirconium-Based Metal–Organic Frameworks. *Acc. Chem. Res.* **2020**, *53*, 1187–1195.
11. Goetjen, T. A.; Liu, J.; Wu, Y.; Sui, J.; Zhang, X.; Hupp, J. T.; Farha, O. K. Metal–Organic Framework (MOF) Materials as Polymerization Catalysts: A Review and Recent Advances. *Chem. Commun.* **2020**, *56*, 10409–10418.
12. Ji, Z.; Li, T.; Yaghi, O. M. Sequencing of Metals in Multivariate Metal–Organic Frameworks. *Science* **2020**, *369*, 674–680.
13. Chen, Z.; Li, P.; Anderson, R.; Wang, X.; Zhang, X.; Robison, L.; Redfern, L. R.; Moribe, S.; Islamoglu, T.; Gómez-Gualdrón, D. A.; Yildirim, T.; Stoddart, J. F.; Farha, O. K. Balancing Volumetric and Gravimetric Uptake in Highly Porous Materials for Clean Energy. *Science* **2020**, *368*, 297–303.
14. Feng, L.; Wang, K. Y.; Willman, J.; Zhou, H. C. Hierarchy in Metal–Organic Frameworks. *ACS Cent. Sci.* **2020**, *6*, 359–367.
15. Islamoglu, T.; Chen, Z.; Wasson, M. C.; Buru, C. T.; Kirlikovali, K. O.; Afrin, U.; Mian, M. R.; Farha, O. K. Metal–Organic Frameworks against Toxic Chemicals. *Chem. Rev.* **2020**, *120*, 8130–8160.
16. Lin, R. B.; Xiang, S.; Zhou, W.; Chen, B. Microporous Metal–Organic Framework Materials for Gas Separation. *Chem* **2020**, *6*, 337–363.
17. Parker, D.; Suturina, E. A.; Kuprov, I.; Chilton, N. F. How the Ligand Field in Lanthanide Coordination Complexes Determines Magnetic Susceptibility Anisotropy, Paramagnetic NMR Shift, and Relaxation Behavior. *Acc. Chem. Res.* **2020**, *53*, 1520–1534.
18. Ramdass, A.; Sathish, V.; Babu, E.; Velayudham, M.; Thanasekaran, P.; Rajagopal, S. Recent Developments on Optical and Electrochemical Sensing of Copper(II) Ion Based on Transition Metal Complexes. *Coord. Chem. Rev.* **2017**, *343*, 278–307.
19. Jiao, K.-J.; Xing, Y.-K.; Yang, Q.-L.; Qiu, H.; Mei, T.-S. Site-Selective C–H Functionalization via Synergistic Use of Electrochemistry and Transition Metal Catalysis. *Acc. Chem. Res.* **2020**, *53*, 300–310.
20. Velazquez, H. D.; Verpoort, F. *N*-Heterocyclic Carbene Transition Metal Complexes for Catalysis in Aqueous Media. *Chem. Soc. Rev.* **2012**, *41*, 7032–7060.

DOI: 10.31635/ccschem.021.202101286
Corrected Citation: *CCS Chem.* **2022**, 4, 755–784
Previous Citation: *CCS Chem.* **2021**, 3, 3436–3465
Link to VoR: https://doi.org/10.31635/ccschem.021.202101286

21. Arrowsmith, R. L.; Pascu, S. I.; Smugowski, H. New Developments in the Biomedical Chemistry of Metal Complexes: From Small Molecules to Nanotheranostic Design. *Organomet. Chem.* **2012**, *38*, 1–35.
22. Ma, D.-L.; He, H.-Z.; Leung, K.-H.; Chan, D. S.-H.; Leung, C.-H. Bioactive Luminescent Transition-Metal Complexes for Biomedical Applications. *Angew. Chem. Int. Ed.* **2013**, *52*, 7666–7682.
23. Ahmedova, A. Biomedical Applications of Metallosupramolecular Assemblies—Structural Aspects of the Anticancer Activity. *Front. Chem.* **2018**, *6*, 620.
24. Ko, C.-N.; Li, G.; Leung, C.-H.; Ma, D.-L. Dual Function Luminescent Transition Metal Complexes for Cancer Theranostics: The Combination of Diagnosis and Therapy. *Coord. Chem. Rev.* **2019**, *381*, 79–103.
25. Colquhoun, H. M.; Stoddart, J. F.; Williams, D. J. Second-Sphere Coordination—A Novel Rôle for Molecular Receptors. *Angew. Chem. Int. Ed. Engl.* **1986**, *25*, 487–507.
26. Raymo, F. M.; Stoddart, J. F. Second-Sphere Coordination. *Chem. Ber.* **1996**, *129*, 981–990.
27. Stoddart, J. F.; Zarzycki, R. Cyclodextrins as Second-Sphere Ligands for Transition Metal Complexes. *Recl. Trav. Chim. Pays-Bas* **1988**, *107*, 515–528.
28. Liu, Z.; Schneebeli, S. T.; Stoddart, J. F. Second-Sphere Coordination Revisited. *Chimia* **2014**, *68*, 315–320.
29. Werner, A. Über Die Raumisomeren Kobaltverbindungen. *Justus Liebigs Ann. Chem.* **1912**, *386*, 1–272.
30. Werner, A. *Neuere Anschauungen Auf Dem Gebiete Der Anorganischen Chemie*; Vieweg: Braunschweig, **1913**.
31. Colquhoun, H. M.; Stoddart, J. F. Second-Sphere Coordination of Neutral and Cationic Transition Metal Complexes by Crown Ethers. *J. Chem. Soc. Chem. Commun.* **1981**, 612–613.
32. Pedersen, C. J. Cyclic Polyethers and Their Complexes with Metal Salts. *J. Am. Chem. Soc.* **1967**, *89*, 2495–2496.
33. Pedersen, C. J. Cyclic Polyethers and Their Complexes with Metal Salts. *J. Am. Chem. Soc.* **1967**, *89*, 7017–7036.
34. Pedersen, C. J. The Discovery of Crown Ethers (Nobel Lecture). *Angew. Chem. Int. Ed. Engl.* **1988**, *27*, 1021–1027.
35. Colquhoun, H. M.; Lewis, D. F.; Stoddart, J. F.; Williams, D. J. Crown Ethers as Second-Sphere Ligands. The Interactions of Transition-Metal Ammines with 18-Crown-6 and Dibenzo-18-Crown-6. *J. Chem. Soc. Dalt. Trans.* **1983**, 607.
36. Colquhoun, H. M.; Stoddart, J. F.; Williams, D. J. Formation and X-Ray Crystal Structure of [Pt$(H_2NCH_2CH_2NH_2)_2$•18-Crown-6]$_n^{2+}$[PF_6]$_{2n}^-$. A Hydrogen Bonded Stepped-Chain Copolymer. *J. Chem. Soc. Chem. Commun.* **1981**, 851–852.
37. Colquhoun, H. M.; Stoddart, J. F.; Williams, D. J. The Binding of Neutral Platinum Complexes by Crown Ethers. X-Ray Crystal Structures of [*trans*-$PtCl_2(PMe_3)NH_3$•Dibenzo-18-Crown-6] and [{*trans*-$PtCl_2(PMe_3)NH_3$}$_2$•18-Crown-6]. *J. Chem. Soc. Chem. Commun.* **1981**, 847–849.
38. Cotton, S. A.; Franckevicius, V.; Mahon, M. F.; Ooi, L. L.; Raithby, P. R.; Teat, S. J. Structures of 2,4,6-Tri-α-Pyridyl-1,3,5-Triazine Complexes of the Lanthanoid Nitrates: A Study in the Lanthanoid Contraction. *Polyhedron* **2006**, *25*, 1057–1068.
39. Colquhoun, H. M.; Stoddart, J. F.; Williams, D. J.; Wolstenholme, J. B.; Zarzycki, R. Second Sphere Coordination of Cationic Platinum Complexes by Crown Ethers—The X-Ray Crystal Structure of [Pt(Bpy)$(NH_3)_2$•Dibenzo[30]Crown-10]$^{2+}$•[PF_6]$_2$.xH_2O (x≈0.6). *Angew. Chem. Int. Ed. Engl.* **1981**, *20*, 1051–1053.
40. Colquhoun, H. M.; Stoddart, J. F.; Williams, D. J. Isolation and X-Ray Crystal Structure of [Cu$(NH_3)_4H_2O$•18-Crown-6]$_n^{2+}$[PF_6]$_{2n}^-$ a Linear Face-to-Face Hydrogen Bonded Chain Copolymer. *J. Chem. Soc. Chem. Commun.* **1981**, 849–850.
41. Colquhoun, H. M.; Stoddart, J. F.; Williams, D. J. Coronation of Ligating Acetonitrile by 18-Crown-6. X-Ray Crystal Structure of {[*trans*-Ir(CO) $(CH_3CN)(PPh_3)_2]^{2+}$•18-Crown-6} [$PF_6]^{2-}$•2CH_2Cl_2. *J. Am. Chem. Soc.* **1982**, *104*, 1426–1428.
42. Colquhoun, H. M.; Doughty, S. M.; Stoddart, J. F.; Williams, D. J. Second Sphere Coordination of Cationic Rhodium Complexes by Dibenzo[3n]Crown-n Ethers. *Angew. Chem. Int. Ed. Engl.* **1984**, *23*, 235–236.
43. Allwood, B. L.; Crosby, J.; Pears, D. A.; Stoddart, J. F.; Williams, D. J. Crown Ether Complexes of Sulfonium Salts—The X-Ray Crystal Structures of [$PhCOCH_2SMe_2$·[18]Crown-6]$_n$[PF_6]$_n$ and [$(PhCOCHPhSMe_2)_2$·[18]Crown-6][PF_6]$_2$. *Angew. Chem. Int. Ed. Engl.* **1984**, *23*, 977–979.
44. Allwood, B. L.; Colquhoun, H. M.; Crosby, J.; Pears, D. A.; Stoddart, J. F.; Williams, D. J. Crown Ether Complexes of Phosphonium Salts—The X-Ray Structure Analysis of [$(Ph_3PMe)_2$·[18]Crown-6][PF_6]$_2$. *Angew. Chem. Int. Ed. Engl.* **1984**, *23*, 824–825.
45. Colquhoun, H. M.; Doughty, S. M.; Slawin, A. M. Z.; Stoddart, J. F.; Williams, D. J. Diamminebis(1,5-cyclooctadiene)(μ-1,4,10,13-tetraoxa-7,16-diazacyclooctadecane-*N*7, *N*16)dirhodiumbis-(hexafluorophosphate): An Example of Simultaneous First and Second Sphere Coordination. *Angew. Chem. Int. Ed. Engl.* **1985**, *24*, 135–136.
46. Alston, D. R.; Slawin, A. M. Z.; Stoddart, J. F.; Williams, D. J.; Zarzycki, R. Second Sphere Coordination of Tetraammineplatinum(II) by a Macropolycyclic Crown Ether Bisamide Receptor. *Angew. Chem. Int. Ed. Engl.* **1987**, *26*, 692–693.
47. Alston, D. R.; Slawin, A. M. Z.; Stoddart, J. F.; Williams, D. J.; Zarzycki, R. Macrobicyclic Polyethers as Second Sphere Ligands for Tetraammineplatinum(II). *Angew. Chem. Int. Ed. Engl.* **1987**, *26*, 693–696.
48. Ballardini, R.; Gandolfi, M. T.; Balzani, V.; Kohnke, F. H.; Stoddart, J. F. Second-Sphere Photochemistry and Photophysics: Luminescence of the [Pt(Bpy)$(NH_3)_2]^2$–Dibenzo [30]Crown-10 Adduct. *Angew. Chem. Int. Ed. Engl.* **1988**, *27*, 692–694.
49. Ballardini, R.; Gandolfi, M. T.; Prodi, L.; Ciano, M.; Balzani, V.; Kohnke, F. H.; Shahriari-Zavareh, H.; Spencer, N.; Stoddart, J. F. Supramolecular Photochemistry and Photophysics. Adducts of Pt(Bpy)$(NH_3)_2^{2+}$ with Aromatic Crown Ethers. *J. Am. Chem. Soc.* **1989**, *111*, 7072–7078.
50. Cameron, B. R.; Corrent, S. S.; Loeb, S. J. Transition Metal Complexes as Both Host and Guest: Second-Sphere Coordination between a Pt-Azacrown Ether Host and a Pt-NH_3 Guest. *Angew. Chem. Int. Ed. Engl.* **1996**, *34*, 2689–2691.

DOI: 10.31635/ccschem.021.202101286
Corrected Citation: *CCS Chem.* **2022**, 4, 755–784
Previous Citation: *CCS Chem.* **2021**, 3, 3436–3465
Link to VoR: https://doi.org/10.31635/ccschem.021.202101286

51. Harada, A.; Takahashi, S. Preparation and Properties of Cyclodextrin–Ferrocene Inclusion Complexes. *J. Chem. Soc. Chem. Commun.* **1984**, 645–646.
52. Alston, D. R.; Stoddart, J. F.; Williams, D. J. The Isolation and X-Ray Structure of an Adduct Formation between 18-Crown-6 and Cisplatin. *J. Chem. Soc. Chem. Commun.* **1985**, *9*, 532–533.
53. Alston, D. R.; Lilley, T. H.; Stoddart, J. F. The Binding of 1,1-Cyclo-Butanedicarboxylatodiammine Platinum(II) by α-Cyclodextrin in Aqueous Solution. *J. Chem. Soc. Chem. Commun.* **1985**, 1600–1602.
54. Alston, D. R.; Slawin, A. M. Z.; Stoddart, J. F.; Williams, D. J. The X-Ray Crystal Structure of a 1:1 Adduct between α-Cyclodextrin and Cyclobutane-1,1-Dicarboxylatodiammine-platinum(II). *J. Chem. Soc. Chem. Commun.* **1985**, 1602–1604.
55. Alston, D. R.; Slawin, A. M. Z.; Stoddart, J. F.; Williams, D. J. Cyclodextrins as Second Sphere Ligands for Transition Metal Complexes—The X-Ray Crystal Structure of [Rh(Cod)$(NH_3)_2$·α-Cyclodextrin][PF_6]·6H_2O. *Angew. Chem. Int. Ed. Engl.* **1985**, *24*, 786–787.
56. Harada, A.; Takahashi, S. Preparation and Properties of Inclusion Compounds of Transition Metal Complexes of Cyclo-Octa-1,5-Diene and Norbornadiene with Cyclodextrins. *J. Chem. Soc. Chem. Commun.* **1986**, 1229.
57. Kamitori, S.; Hirotsu, K.; Higuchi, T. Crystal and Molecular Structures of Double Macrocyclic Inclusion Complexes Composed of Cyclodextrins, Crown Ethers, and Cations. *J. Am. Chem. Soc.* **1987**, *109*, 2409–2414.
58. Alston, D. R.; Slawin, A. M. Z.; Stoddart, J. F.; Williams, D. J.; Zarzycki, R. Second Sphere Coordination Adducts of Phosphane-Transition Metal Complexes with β-Cyclodextrin and Its Methylated Derivative. *Angew. Chem. Int. Ed. Engl.* **1988**, *27*, 1184–1185.
59. Alston, D. R.; Ashton, P. R.; Lilley, T. H.; Fraser Stoddart, J.; Zarzycki, R.; Slawin, A. M. Z.; Williams, D. J. Second-Sphere Co-Ordination of Carboplatin and Rhodium Complexes by Cyclodextrins (Cyclomalto-Oligosaccharides). *Carbohydr. Res.* **1989**, *192*, 259–281.
60. Harada, A.; Yamamoto, S.; Takahashi, S. Preparation and Properties of Inclusion Compounds of Transition-Metal Complexes of Cycloocta-1,5-diene and Norbornadiene with Cyclodextrins. *Organometallics* **1989**, *8*, 2560–2563.
61. Harada, A.; Shimada, M.; Takahashi, S. γ-Cyclodextrin as a Second Sphere Coordinating Ligand for Cobalt Cluster Complexes. *Chem. Lett.* **1989**, *18*, 275–276.
62. Ando, I.; Ujimoto, K.; Kurihara, H. Effect of Second-Sphere Coordination 9. Partial Inclusion of Pentaamminer-uthenium(II) and Pentacyanoferrate(II) Complexes with Nitrogen Heterocycles into a Cyclodextrin Cavity. *Bull. Chem. Soc. Jpn.* **2001**, *74*, 717–721.
63. Engeldinger, E.; Armspach, D.; Matt, D.; Jones, P. G.; Welter, R. A Cyclodextrin Diphosphane as a First and Second Coordination Sphere Cavitand: Evidence for Weak C-H ···Cl–M Hydrogen Bonds within Metal-Capped Cavities. *Angew. Chem. Int. Ed.* **2002**, *41*, 2593–2596.
64. Engeldinger, E.; Armspach, D.; Matt, D.; Jones, P. G. Cyclodextrin Phosphanes as First and Second Coordination Sphere Cavitands. *Chem. Eur. J.* **2003**, *9*, 3091–3105.
65. Liu, Y.; Zhong, R.-Q.; Zhang, H.-Y.; Song, H.-B. A Unique Tetramer of 4:5 β-Cyclodextrin-Ferrocene in the Solid State. *Chem. Commun.* **2005**, 2211–2213.
66. Atwood, J. L.; Orr, G. W.; Hamada, F.; Vincent, R. L.; Bott, S. G.; Robinson, K. D. Second-Sphere Coordination of Transition-Metal Complexes by Calix[4]Arenes. *J. Am. Chem. Soc.* **1991**, *113*, 2760–2761.
67. Atwood, J. L.; Orr, G. W.; Hamada, F.; Vincent, R. L.; Bott, S. G.; Robinson, K. D. Calixarenes as Second-Sphere Ligands for Transition Metal Ions. Synthesis and Crystal Structure of [$(H_2O)_5Ni(NC_5H_5)]_2$(Na)[Calix[4]arene Sulfonate]•3.5 H_2O and [$(H_2O)_4Cu(NC_5H_5)_2](H_3O)_3$ [Calix[4]arene Sulfonate]•10 H_2O. *J. Incl. Phenom. Mol. Recognit. Chem.* **1992**, *14*, 37–46.
68. Atwood, J. L.; Orr, G. W.; Robinson, K. D. First Structural Authentication of Third-Sphere Coordination: [P-Sulfonato-calix[*4*]arene]$^{5-}$ as a Third-Sphere Ligand for Eu^{3+}. *Supramol. Chem.* **1994**, *3*, 89–91.
69. Beer, P. D.; Drew, M. G. B.; Ogden, M. I. First- and Second-Sphere Co-ordination of a Lanthanum Cation by a Calix[*4*]arene Tetraamide in the Partial-Cone Conformation. *J. Chem. Soc. Dalt. Trans.* **1997**, 1489–1492.
70. Junk, P. C.; Atwood, J. L. Use of Metal Carbonyls in the Formation of [$H_5O_2^+$·15-Crown-5][$MOCl_4(H_2O)^-$], (M=Mo, W), and a Second Sphere Coordination Complex in [*mer*-$CrCl_3(H_2O)_3$·15-Crown-5]. *J. Organomet. Chem.* **1998**, *565*, 179–186.
71. Belhamel, K.; Nguyen, T. K. D.; Benamor, M.; Ludwig, R. Design of Calixarene-Type Ligands for Second Sphere Complexation of Noble Metal Ions. *Eur. J. Inorg. Chem.* **2003**, *2003*, 4110–4116.
72. MacGillivray, L. R.; Spinney, H. A.; Reid, J. L.; Ripmeester, J. A. Entrapment of Ferrocenes within Supramolecular, Deep-Cavity Resorcin[4]arenes. *Chem. Commun.* **2000**, 517–518.
73. Shen, L.; Zhao, Y.; Dai, D.; Yang, Y.-W.; Wu, B.; Yang, X.-J. Stabilization of Grignard Reagents by A Pillar[*5*]arene Host—Schlenk Equilibria and Grignard Reactions. *Chem. Commun.* **2020**, *56*, 1381–1384.
74. Thuéry, P. Lanthanide Complexes with Cucurbit[*n*]uril (n = 5, 6, and 7) and Perrhenate Ligands: New Examples of Encapsulation of Perrhenate Anions. *Inorg. Chem.* **2009**, *48*, 4497–4513.
75. Quan, M. L. C.; Cram, D. J. Constrictive Binding of Large Guests by a Hemicarcerand Containing Four Portals. *J. Am. Chem. Soc.* **1991**, *113*, 2754–2755.
76. Ashton, P. R.; Claessens, C. G.; Hayes, W.; Stoddart, J. F.; Menzer, S.; White, A. J. P.; Williams, D. J. Molecular Mosaics Formed by a Square Cyclophane and Its Inclusion Complex with Ferrocene. *Angew. Chem. Int. Ed. Engl.* **1995**, *34*, 1862–1865.
77. Ashton, P. R.; Menzer, S.; Raymo, F. M.; Shimizu, G. K. H.; Stoddart, J. F.; Williams, D. J. The Template-Directed Synthesis of Cyclobis(paraquat-4,4′-biphenylene). *Chem. Commun.* **1996**, 487–490.
78. Raymo, F. M.; Stoddart, J. F. Self-Assembling Cyclobis (paraquat-4,4′-biphenylene). *Pure Appl. Chem.* **1996**, *68*, 313–322.

DOI: 10.31635/ccschem.021.202101286
Corrected Citation: *CCS Chem.* **2022**, 4, 755–784
Previous Citation: *CCS Chem.* **2021**, 3, 3436–3465
Link to VoR: https://doi.org/10.31635/ccschem.021.202101286

79. Asakawa, M.; Ashton, P. R.; Menzer, S.; Raymo, F. M.; Stoddart, J. F.; White, A. J. P.; Williams, D. J. Cyclobis(paraquat-4,4′-biphenylene)—An Organic Molecular Square. *Chem. Eur. J.* **1996**, *2*, 877–893.
80. Kickham, J. E.; Loeb, S. J.; Murphy, S. L. Molecular Recognition of Nucleobases via Simultaneous First- and Second-Sphere Coordination. *J. Am. Chem. Soc.* **1993**, *115*, 7031–7032.
81. Kickham, J. E.; Loeb, S. J. Simultaneous First- and Second-Sphere Coordination. Organopalladium Metalloreceptors for Water, Ammonia, Amines, Hydrazine, and the Hydrazinium Ion. *Inorg. Chem.* **1995**, *34*, 5656–5665.
82. Kickham, J. E.; Loeb, S. J. Simultaneous First- and Second-Sphere Coordination. Organopalladium Crown Ether Complexes as Metalloreceptors for *o*-Aminopyridine Derivatives. *Inorg. Chem.* **1994**, *33*, 4351–4359.
83. Kickham, J. E.; Loeb, S. J. Receptors for the Hydrazinium Ion. Simultaneous First- and Second-Sphere Coordination inside Organopalladium Crown Ether Complexes. *J. Chem. Soc. Chem. Commun.* **1993**, 1848–1850.
84. Steed, J. W. First- and Second-Sphere Coordination Chemistry of Alkali Metal Crown Ether Complexes. *Coord. Chem. Rev.* **2001**, *215*, 171–221.
85. Beauchamp, D. A.; Loeb, S. J. Hydrogen-Bonded Networks through Second-Sphere Coordination. *Chem. Eur. J.* **2002**, *8*, 5084–5088.
86. Mercer, D. J.; Loeb, S. J. Metal-Based Anion Receptors: An Application of Second-Sphere Coordination. *Chem. Soc. Rev.* **2010**, *39*, 3612–3620.
87. Zhao, M.; Wang, H.-B.; Ji, L.-N.; Mao, Z.-W. Insights into Metalloenzyme Microenvironments: Biomimetic Metal Complexes with a Functional Second Coordination Sphere. *Chem. Soc. Rev.* **2013**, *42*, 8360–8375.
88. Guo, F.; Martí-Rujas, J. Second Sphere Coordination of Hybrid Metal-Organic Materials: Solid State Reactivity. *Dalton Trans.* **2016**, *45*, 13648–13662.
89. Therrien, B. The Role of the Second Coordination Sphere in the Biological Activity of Arene Ruthenium Metalla-Assemblies. *Front. Chem.* **2018**, *6*, 1–7.
90. Shaffer, C. C.; Smith, B. D. Macrocyclic and Acyclic Supramolecular Elements for Co-Precipitation of Square-Planar Gold(III) Tetrahalide Complexes. *Org. Chem. Front.* **2021**, *8*, 1294–1301.
91. Liu, W.; Stoddart, J. F. Emergent Behavior in Nanoconfined Molecular Containers. *Chem* **2021**, *7*, 919–947.
92. Liu, W.; Samanta, S. K.; Smith, B. D.; Isaacs, L. Synthetic Mimics of Biotin/(Strept)Avidin. *Chem. Soc. Rev.* **2017**, *46*, 2391–2403.
93. Cameron, B. R.; Loeb, S. J.; Yap, G. P. A. Calixarene Metalloreceptors. Synthesis and Molecular Recognition Properties of Upper-Rim Functionalized Calix[4]arenes Containing an Organopalladium Binding Site. *Inorg. Chem.* **1997**, *36*, 5498–5504.
94. Kickham, J. E.; Loeb, S. J.; Murphy, S. L. Molecular Receptors for Adenine and Guanine Employing Metal Coordination, Hydrogen-Bonding and π-Stacking Interactions. *Chem. Eur. J.* **1997**, *3*, 1203–1213.
95. Horeau, M.; Lautrette, G.; Wicher, B.; Blot, V.; Lebreton, J.; Pipelier, M.; Dubreuil, D.; Ferrand, Y.; Huc, I. Metal-Coordination-Assisted Folding and Guest Binding in Helical Aromatic Oligoamide Molecular Capsules. *Angew. Chem. Int. Ed.* **2017**, *129*, 6927–6931.
96. Mateus, P.; Wicher, B.; Ferrand, Y.; Huc, I. Alkali and Alkaline Earth Metal Ion Binding by a Foldamer Capsule: Selective Recognition of Magnesium Hydrate. *Chem. Commun.* **2017**, *53*, 9300–9303.
97. Mateus, P.; Wicher, B.; Ferrand, Y.; Huc, I. Carbohydrate Binding through First- and Second-Sphere Coordination within Aromatic Oligoamide Metallofoldamers. *Chem. Commun.* **2018**, *54*, 5078–5081.
98. Meunier, A.; Singleton, M. L.; Kauffmann, B.; Granier, T.; Lautrette, G.; Ferrand, Y.; Huc, I. Aromatic Foldamers as Scaffolds for Metal Second Coordination Sphere Design. *Chem. Sci.* **2020**, *11*, 12178–12186.
99. Zhang, L.; Stephens, A. J.; Lemonnier, J. F.; Pirvu, L.; Vitorica-Yrezabal, I. J.; Robinson, C. J.; Leigh, D. A. Coordination Chemistry of a Molecular Pentafoil Knot. *J. Am. Chem. Soc.* **2019**, *141*, 3952–3958.
100. Ayme, J.-F.; Beves, J. E.; Campbell, C. J.; Gil-Ramírez, G.; Leigh, D. A.; Stephens, A. J. Strong and Selective Anion Binding within the Central Cavity of Molecular Knots and Links. *J. Am. Chem. Soc.* **2015**, *137*, 9812–9815.
101. Marcos, V.; Stephens, A. J.; Jaramillo-Garcia, J.; Nussbaumer, A. L.; Woltering, S. L.; Valero, A.; Lemonnier, J. F.; Vitorica-Yrezabal, I. J.; Leigh, D. A. Allosteric Initiation and Regulation of Catalysis with a Molecular Knot. *Science* **2016**, *352*, 1555–1559.
102. Fielden, S. D. P.; Leigh, D. A.; Woltering, S. L. Molecular Knots. *Angew. Chem. Int. Ed.* **2017**, *56*, 11166–11194.
103. Stoddart, J. F. Mechanically Interlocked Molecules (MIMs)–Molecular Shuttles, Switches, and Machines (Nobel Lecture). *Angew. Chem. Int. Ed.* **2017**, *56*, 11904–11125.
104. Bruns, C. J.; Stoddart, J. F. *The Nature of the Mechanical Bond*; Wiley: Hoboken, NJ, **2016**.
105. Stoddart, J. F. The Chemistry of the Mechanical Bond. *Chem. Soc. Rev.* **2009**, *38*, 1802–1820.
106. Stoddart, J. F.; Colquhoun, H. M. Big and Little Meccano. *Tetrahedron* **2008**, *64*, 8231–8263.
107. Philp, D.; Stoddart, J. F. Self-Assembly in Natural and Unnatural Systems. *Angew. Chem. Int. Ed. Engl.* **1996**, *35*, 1155–1196.
108. Amabilino, D. B.; Stoddart, J. F. Interlocked and Intertwined Structures and Superstructures. *Chem. Rev.* **1995**, *95*, 2725–2828.
109. Stoddart, J. F. Putting Mechanically Interlocked Molecules (MIMs) to Work in Tomorrow's World. *Angew. Chem. Int. Ed.* **2014**, *53*, 11102–11104.
110. Wasserman, E. The Preparation of Interlocking Rings: A Catenane. *J. Am. Chem. Soc.* **1960**, *82*, 4433–4434.
111. Schill, G.; Lüttringhaus, A. The Preparation of Catena Compounds by Directed Synthesis. *Angew. Chem. Int. Ed.* **1964**, *3*, 546–547.
112. Dietrich-Buchecker, C. O.; Sauvage, J.-P.; Kintzinger, J.-P. Une Nouvelle Famille de Molecules: Les Metallo-Catenanes. *Tetrahedron Lett.* **1983**, *24*, 5095–5098.

DOI: 10.31635/ccschem.021.202101286
Corrected Citation: *CCS Chem.* **2022**, 4, 755–784
Previous Citation: *CCS Chem.* **2021**, 3, 3436–3465
Link to VoR: https://doi.org/10.31635/ccschem.021.202101286

113. Johnston, A. G.; Leigh, D. A.; Pritchard, R. J.; Deegan, M. D. Facile Synthesis and Solid-State Structure of a Benzylic Amide [2]Catenane. *Angew. Chem. Int. Ed.* **1995**, *34*, 1209–1212.
114. Johnston, A. G.; Leigh, D. A.; Nezhat, L.; Smart, J. P.; Deegan, M. D. Structurally Diverse and Dynamically Versatile Benzylic Amide [2]Catenanes Assembled Directly from Commercially Available Precursors. *Angew. Chem. Int. Ed.* **1995**, *34*, 1212–1216.
115. Asakawa, M.; Ashton, P. R.; Balzani, V.; Credi, A.; Hamers, C.; Mattersteig, G.; Montalti, M.; Shipway, A. N.; Spencer, N.; Stoddart, J. F.; Tolley, M. S.; Venturi, M.; White, A. J. P.; Williams, D. J. A Chemically and Electrochemically Switchable [2]Catanane Incorporating a Tetrathiafulvalent Unit. *Angew. Chem. Int. Ed.* **1998**, *37*, 333–337.
116. Sauvage, J.-P. From Chemical Topology to Molecular Machines (Nobel Lecture). *Angew. Chem. Int. Ed.* **2017**, *56*, 11080–11093.
117. Fujita, M.; Ogura, K. Supramolecular Self-Assembly of Macrocycles, Catenanes, and Cages through Coordination of Pyridine-Based Ligands to Transition Metals. *Bull. Chem. Soc. Jpn.* **1996**, *69*, 1471–1482.
118. Nepogodiev, S. A.; Stoddart, J. F. Cyclodextrin-Based Catenanes and Rotaxanes. *Chem. Rev.* **1998**, *98*, 1959–1976.
119. Fujita, M. Self-Assembly of [2]Catenanes Containing Metals in Their Backbones. *Acc. Chem. Res.* **1999**, *32*, 53–61.
120. Faiz, J. A.; Heitz, V.; Sauvage, J.-P. Design and Synthesis of Porphyrin-Containing Catenanes and Rotaxanes. *Chem. Soc. Rev.* **2009**, *38*, 422–442.
121. Wu, Q.; Rauscher, P. M.; Lang, X.; Wojtecki, R. J.; de Pablo, J. J.; Hore, M. J. A.; Rowan, S. J. Poly[n]Catenanes: Synthesis of Molecular Interlocked Chains. *Science* **2017**, *358*, 1434–1439.
122. Erbas-Cakmak, S.; Fielden, S. D. P.; Karaca, U.; Leigh, D. A.; McTernan, C. T.; Tetlow, D. J.; Wilson, M. R. Rotary and Linear Molecular Motors Driven by Pulses of a Chemical Fuel. *Science* **2017**, *358*, 340–343.
123. Harrison, I. T.; Harrison S. The Synthesis of a Stable Complex of a Macrocycle and a Threaded Chain. *J. Am. Chem. Soc.* **1967**, *89*, 5723–5724.
124. Schill, G.; Zollenkopf, H. Rotaxane–Verbindungen, I. *Liebigs Ann. Chem.* **1969**, *721*, 53–74.
125. Anelli, P. L.; Spencer, N.; Stoddart J. F. A Molecular Shuttle. *J. Am. Chem. Soc.* **1991**, *113*, 5131–5133.
126. Gassensmith, J. J.; Baumes, J. M.; Smith, B. D. Discovery and Early Development of Squaraine Rotaxanes. *Chem. Commun.* **2009**, 6329–6338.
127. Bruns, C. J.; Stoddart, J. F. Rotaxane-Based Molecular Muscles. *Acc. Chem. Res.* **2014**, *47*, 2186–2199.
128. Durola, F.; Heitz, V.; Reviriego, F.; Roche, C.; Sauvage, J.-P.; Sour, A.; Trolez, Y. Cyclic [4]Rotaxanes Containing Two Parallel Porphyrinic Plates: Toward Switchable Molecular Receptors and Compressors. *Acc. Chem. Res.* **2014**, *47*, 633–645.
129. Langton, M. J.; Beer, P. D. Rotaxane and Catenane Host Structures for Sensing Charged Guest Species. *Acc. Chem. Res.* **2014**, *47*, 1935–1949.
130. Leigh, D. A.; Marcos, V.; Wilson, M. R. Rotaxane Catalysts. *ACS Catal.* **2014**, *4*, 4490–4497.
131. van Dongen, S. F. M.; Elemans, J. A. A. W.; Rowan, A. E.; Nolte, R. J. M. Processive Catalysis. *Angew. Chem. Int. Ed.* **2014**, *53*, 11420–11428.
132. Hashidzume, A.; Yamaguchi, H.; Harada, A. Cyclodextrin-Based Rotaxanes: From Rotaxanes to Polyrotaxanes and Further to Functional Materials. *Eur. J. Org. Chem.* **2019**, *2019*, 3344–3357.
133. Northrop, B. H.; Aricó, F.; Tangchiavang, N.; Badjić, J. D.; Stoddart, J. F. Template-Directed Synthesis of Mechanically Interlocked Molecular Bundles Using Dynamic Covalent Chemistry. *Org. Lett.* **2006**, *8*, 3899–3902.
134. Williams, A. R.; Northrop, B. H.; Chang, T.; Stoddart, J. F.; White, A. J. P.; Williams, D. J. Suitanes. *Angew. Chem. Int. Ed.* **2006**, *45*, 6665–6669.
135. Pun, A.; Hanifi, D. A.; Kiel, G.; O'Brien, E.; Liu, Y. Facile Route to an All-Organic, Triply Threaded, Interlocked Structure by Templated Dynamic Clipping. *Angew. Chem. Int. Ed.* **2012**, *51*, 13119–13122.
136. Zhu, K.; Baggi, G.; Vukotic, V. N.; Loeb, S. J. Reversible Mechanical Protection: Building a 3D "Suit" around a T-Shaped Benzimidazole Axle. *Chem. Sci.* **2017**, *8*, 3898–3904.
137. Liu, W.; Stern, C. L.; Stoddart, J. F. Suit[4]ane. *J. Am. Chem. Soc.* **2020**, *142*, 10273–10278.
138. Chen, X. Y.; Shen, D.; Cai, K.; Jiao, Y.; Wu, H.; Song, B.; Zhang, L.; Tan, Y.; Wang, Y.; Feng, Y.; Stern, C. L.; Stoddart, J. F. Suit[3]ane. *J. Am. Chem. Soc.* **2020**, *142*, 20152–20160.
139. Xu, H.; Lin, M.-D.; Yuan, J.; Zhou, B.; Mu, Y.; Huo, Y.; Zhu, K. Fluorescence Emission Enhancement of a T-Shaped Benzimidazole with a Mechanically-Interlocked 'Suit.' *Chem. Commun.* **2021**, *57*, 3239–3242.
140. Balzani, V.; Credi, A.; Raymo, F. M.; Stoddart, J. F. Artificial Molecular Machines. *Angew. Chem. Int. Ed.* **2000**, *39*, 3348–3391.
141. Collin, J.-P.; Heitz, V.; Bonnet, S.; Sauvage, J.-P. Transition Metal-Complexed Catenanes and Rotaxanes in Motion: Towards Molecular Machines. *Inorg. Chem. Commun.* **2005**, *8*, 1063–1074.
142. Browne, W. R.; Feringa, B. L. Making Molecular Machines Work. *Nat. Nanotechnol.* **2006**, *1*, 25–35.
143. Coskin, A.; Banaszak, M.; Astumian, R. D.; Stoddart, J. F.; Grzybowski, B. A. Great Expectations: Can Artificial Molecular Machines Deliver on Their Promise? *Chem. Soc. Rev.* **2012**, *41*, 19–30.
144. Qiu, Y.; Feng, Y.; Guo, Q.-H.; Astumian, R. D.; Stoddart, J. F. Pumps through the Ages. *Chem* **2020**, *6*, 1952–1977.
145. Feng, Y.; Ovalle, M.; Seale, J. S. W.; Lee, C. K.; Kim, D. J.; Stoddart, J. F. Molecular Pumps and Motors. *J. Am. Chem. Soc.* **2021**. *143*, 5569–5591.
146. Lewandowski, B.; De Bo, G.; Ward, J. W.; Papmeyer, M.; Kuschel, S.; Aldegunde, M. J.; Gramlich, P. M. E.; Heckmann, D.; Goldup, S. M.; Souza, D. M.; Fernandes, A. E.; Leigh, D. A. Sequence-Specific Peptide Synthesis by an Artificial Small-Molecule Machine. *Science* **2013**, *339*, 189–193.
147. Cheng, C.; Stoddart, J. F. Wholly Synthetic Molecular Machines. *ChemPhysChem* **2016**, *17*, 1780–1793.

DOI: 10.31635/ccschem.021.202101286
Corrected Citation: *CCS Chem.* **2022**, 4, 755–784
Previous Citation: *CCS Chem.* **2021**, 3, 3436–3465
Link to VoR: https://doi.org/10.31635/ccschem.021.202101286

148. Wilson, M. R.; Solà, J.; Carlone, A.; Goldup, S. M.; Lebrasseur, N.; Leigh, D. A. An Autonomous Chemically Fuelled Small-Molecule Motor. *Nature* **2016**, *534*, 235–240.
149. Pezzato, C.; Cheng, C.; Stoddart, J. F.; Astumian, R. D. Mastering the Non-Equilibrium Assembly and Operation of Molecular Machines. *Chem. Soc. Rev.* **2017**, *46*, 5491–5507.
150. Kassem, S.; Lee, A. T. L.; Leigh, D. A.; Marcos, V.; Palmer, L. I.; Pisano, S. Stereodivergent Synthesis with a Programmable Molecular Machine. *Nature* **2017**, *549*, 374–378.
151. Wang, Y.; Frasconi, M.; Stoddart, J. F. Introducing Stable Radicals into Molecular Machines. *ACS Cent. Sci.* **2017**, *3*, 927–935.
152. Qiu, Y.; Song, B.; Pezzato, C.; Shen, D.; Liu, W.; Zhang, L.; Feng, Y.; Guo, Q. H.; Cai, K.; Li, W.; Chen, H.; Nguyen, M. T.; Shi, Y.; Cheng, C.; Dean Astumian, R.; Li, X.; Stoddart, J. F. A Precise Polyrotaxane Synthesizer. *Science* **2020**, *368*, 1247–1253.
153. Corra, S.; Curcio, M.; Baroncini, M.; Silvi, S.; Credi, A. Photoactivated Artificial Molecular Machines that Can Perform Tasks. *Adv. Mater.* **2020**, *32*, 1906064.
154. Vickers, M. S.; Beer, P. D. Anion Templated Assembly of Mechanically Interlocked Structures. *Chem. Soc. Rev.* **2007**, *36*, 211–225.
155. Griffiths, K. E.; Stoddart, J. F. Template-Directed Synthesis of Donor/Acceptor [2]Catenanes and [2]Rotaxanes. *Pure Appl. Chem.* **2008**, *80*, 485–506.
156. Mullen, K. M.; Beer, P. D. Sulfate Anion Templation of Macrocycles, Capsules, Interpenetrated and Interlocked Structures. *Chem. Soc. Rev.* **2009**, *38*, 1701–1713.
157. Crowley, J. D.; Goldup, S. M.; Lee, A.-L.; Leigh, D. A.; McBurney, R. T. Active Metal Template Synthesis of Rotaxanes, Catenanes and Molecular Shuttles. *Chem. Soc. Rev.* **2009**, *38*, 1530–1541.
158. Aucagne, V.; Hänni, K. D.; Leigh, D. A.; Lusby, P. J.; Walker, D. B. Catalytic "Click" Rotaxanes: A Substoichiometric Metal-Template Pathway to Mechanically Interlocked Architectures. *J. Am. Chem. Soc.* **2006**, *128*, 2186–2187.
159. Saito, S.; Takahashi, E.; Nakazono, K. Synthesis of [2] Rotaxanes by the Catalytic Reactions of a Macrocyclic Copper Complex. *Org. Lett.* **2006**, *8*, 5133–5136.
160. Crowley, J. D.; Hänni, K. D.; Lee, A.-L.; Leigh, D. A. [2] Rotaxanes through Palladium Active-Template Oxidative Heck Cross-Couplings. *J. Am. Chem. Soc.* **2007**, *129*, 12092–12093.
161. Berná, J.; Crowley, J. D.; Goldup, S. M.; Hänni, K. D.; Lee, A.-L.; Leigh, D. A. A Catalytic Palladium Active-Metal Template Pathway to [2]Rotaxanes. *Angew. Chem. Int. Ed.* **2007**, *46*, 5709–5713.
162. Aucagne, V.; Berná, J.; Crowley, J. D.; Goldup, S. M.; Hänni, K. D.; Leigh, D. A.; Lusby, P. J.; Ronaldson, V. E.; Slawin, A. M. Z.; Viterisi, A.; Walker, D. B. Catalytic "Active-Metal" Template Synthesis of [2]Rotaxanes, [3]Rotaxanes, and Molecular Shuttles, and Some Observations on the Mechanism of the Cu(I)-Catalyzed Azide–Alkyne 1,3-Cycloaddition. *J. Am. Chem. Soc.* **2007**, *129*, 11950–11963.
163. Sato, Y.; Yamasaki, R.; Saito, S. Synthesis of [2]Catenanes by Oxidative Intramolecular Diyne Coupling Mediated by Macrocyclic Copper(I) Complexes. *Angew. Chem. Int. Ed.* **2009**, *48*, 504–507.
164. Goldup, S. M.; Leigh, D. A.; Long, T.; McGonigal, P. R.; Symes, M. D.; Wu, J. Active Metal Template Synthesis of [2] Catenanes. *J. Am. Chem. Soc.* **2009**, *131*, 15924–15929.
165. Barran, P. E.; Cole, H. L.; Goldup, S. M.; Leigh, D. A.; McGonigal, P. R.; Symes, M. D.; Wu, J.; Zengerle, M. Active-Metal Template Synthesis of a Molecular Trefoil Knot. *Angew. Chem. Int. Ed.* **2011**, *50*, 12280–12284.
166. Ibukuro, F.; Fujita, M.; Yamaguchi, K.; Sauvage, J.-P. Quantitative and Spontaneous Formation of a Doubly Interlocking [2]Catenane Using Copper(I) and Palladium(II) as Templating and Assembling Centers. *J. Am. Chem. Soc.* **1999**, *121*, 11014–11015.
167. Dietrich-Buchecker, C.; Colasson, B.; Fujita, M.; Hori, A.; Geum, N.; Sakamoto, S.; Yamaguchi, K.; Sauvage, J.-P. Quantitative Formation of [2]Catenanes Using Copper(I) and Palladium(II) as Templating and Assembling Centers: The Entwining Route and the Threading Approach. *J. Am. Chem. Soc.* **2003**, *125*, 5717–5725.
168. Liu, Y.; Zhao, Y.; Sun, X.; Furukawa, H.; Ma, Y.; Oleynikov, P.; Gandara, F.; Liu, Z.; Suenaga, K.; Zhu, H.; Zhu, C.; Alshammari, A. S.; Zhang, X.; Terasaki, O.; Yaghi, O. M. Weaving of Organic Threads into a Crystalline Covalent Organic Framework. *Science* **2016**, *351*, 365–369.
169. Blight, B. A.; Van Noortwyk, K. A.; Wisner, J. A.; Jennings, M. C. [2]Pseudorotaxanes Through Second-Sphere Coordination. *Angew. Chem. Int. Ed.* **2005**, *44*, 1499–1504.
170. Blight, B. A.; Wisner, J. A.; Jennings, M. C. Synthesis of a [2]Rotaxane through First- and Second-Sphere Coordination. *Chem. Commun.* **2006**, 4593–4595.
171. Blight, B. A.; Wei, X.; Wiener, J. A.; Jennings, M. C. [2] Pseudorotaxane and [2]Rotaxane Molecular Shuttles: Self-Assembly through Second-Sphere Coordination of Thiocyanate Ligands. *Inorg. Chem.* **2007**, *46*, 8445–8447.
172. Blight, B. A.; Wisner, J. A.; Jennings, M. C. Stability of [2] Pseudorotaxanes Templated through Second-Sphere Coordination. *Inorg. Chem.* **2009**, *48*, 1920–1927.
173. Blight, B. A.; Wisner, J. A.; Jennings, M. C. Reversible Formation of a [2]Catenane through First- and Second-Sphere Coordination. *Angew. Chem. Int. Ed.* **2007**, *46*, 2835–2838.
174. Amini, M. M.; Rheingold, A. L.; Taylor, R. W.; Zuckerman, J. J. A New Environment for Water. The First Authenticated Example of Water Molecules Engaged in Twin, Three-Center Hydrogen Bonds: The Crystal and Molecular Structure of $\{[(CH_3)_2SnCl_2 \bullet H_2O]_2 \bullet 18\text{-Crown-}6\}_n$. *J. Am. Chem. Soc.* **1984**, *106*, 7289–7291.
175. Zhu, X.; Ma, Z.; Bi, W.; Wang, Y.; Yuan, D.; Cao R. Formation of a Sandwich-Type Supercomplex through Second-Sphere Coordination of Functionalized Macrocyclic Polyamines. *CrystEngComm* **2008**, *10*, 19–22.
176. Dalrymple, S. A.; Parvez, M.; Shimizu, G. K. H. Supramolecular Encapsulation of Hexaaquo Metal Ions by Second Sphere Coordination. *Chem. Commun.* **2001**, 2672–2673.
177. Dalrymple, S. A.; Parvez, M.; Shimizu, G. K. H. Intra- and Intermolecular Second-Sphere Coordination Chemistry: Formation of Capsules, Half-Capsules, and Extended

DOI: 10.31635/ccschem.021.202101286
Corrected Citation: *CCS Chem.* **2022**, 4, 755–784
Previous Citation: *CCS Chem.* **2021**, 3, 3436–3465
Link to VoR: https://doi.org/10.31635/ccschem.021.202101286

Structures with Hexaaquo- and Hexaamminemetal Ions. *Inorg. Chem.* **2002**, *41*, 6986–6996.
178. Dalrymple, S. A.; Shimizu, G. K. H. Exploiting Complementary Second-Sphere Effects in Supramolecular Coordination Solids. *Supramol. Chem.* **2003**, *15*, 591–606.
179. Dalrymple, S. A.; Shimizu, G. K. H. An Open Channel Coordination Framework Sustained by Cooperative Primary and Secondary Sphere Interactions. *Chem. Commun.* **2002**, 2224–2225.
180. Reddy, D. S.; Duncan, S.; Shimizu, G. A Family of Supramolecular Inclusion Solids Based Upon Second-Sphere Interactions. *Angew. Chem.* **2003**, *115*, 1398–1402.
181. Taylor, J. M.; Dwyer, P. J.; Reid, J. W.; Gelfand, B. S.; Lim, D. woon; Donoshita, M.; Veinberg, S. L.; Kitagawa, H.; Vukotic, V. N.; Shimizu, G. K. H. Holding Open Micropores with Water: Hydrogen-Bonded Networks Supported by Hexaaquachromium(III) Cations. *Chem* **2018**, *4*, 868–878.
182. Ubaldini, S.; Massidda, R.; Vegliò, F.; Beolchini, F. Gold Stripping by Hydro-Alcoholic Solutions from Activated Carbon: Experimental Results and Data Analysis by a Semi-Empirical Model. *Hydrometallurgy* **2006**, *81*, 40–44.
183. Soleimani, M.; Kaghazchi, T. Gold Recovery from Loaded Activated Carbon Using Different Solvents. *J. Chin. Inst. Chem. Eng.* **2008**, *39*, 9–11.
184. Bunney, K.; Jeffrey, M. I.; Pleysier, R.; Breuer, P. L. Selective Elution of Gold, Silver and Mercury Cyanide from Activated Carbon. *Miner. Metall. Process.* **2010**, *27*, 205–211.
185. Liu, W.; Jones, L. O.; Wu, H.; Stern, C. L.; Sponenburg, R. A.; Schatz, G. C.; Stoddart, J. F. Supramolecular Gold Stripping from Activated Carbon Using α-Cyclodextrin. *J. Am. Chem. Soc.* **2021**, *143*, 1984–1992.
186. Liu, Z.; Frasconi, M.; Lei, J.; Brown, Z. J.; Zhu, Z.; Cao, D.; Iehl, J.; Liu, G.; Fahrenbach, A. C.; Botros, Y. Y.; Farha, O. K.; Hupp, J. T.; Mirkin, C. A.; Stoddart, J. F. Selective Isolation of Gold Facilitated by Second-Sphere Coordination with α-Cyclodextrin. *Nat. Commun.* **2013**, *4*, 1855.
187. Liu, Z.; Samanta, A.; Lei, J.; Sun, J.; Wang, Y.; Stoddart, J. F. Cation-Dependent Gold Recovery with α-Cyclodextrin Facilitated by Second-Sphere Coordination. *J. Am. Chem. Soc.* **2016**, *138*, 11643–11653.
188. Smaldone, R. A.; Forgan, R. S.; Furukawa, H.; Gassensmith, J. J.; Slawin, A. M. Z.; Yaghi, O. M.; Stoddart, J. F. Metal–Organic Frameworks from Edible Natural Products. *Angew. Chem. Int. Ed.* **2010**, *49*, 8630–8634.
189. Gassensmith, J. J.; Furukawa, H.; Smaldone, R. A.; Forgan, R. S.; Botros, Y. Y.; Yaghi, O. M.; Stoddart, J. F. Strong and Reversible Binding of Carbon Dioxide in a Green Metal–Organic Framework. *J. Am. Chem. Soc.* **2011**, *133*, 15312–15315.
190. Forgan, R. S.; Smaldone, R. A.; Gassensmith, J. J.; Furukawa, H.; Cordes, D. B.; Li, Q.; Wilmer, C. E.; Botros, Y. Y.; Snurr, R. Q.; Slawin, A. M. Z.; Stoddart, J. F. Nanoporous Carbohydrate Metal–Organic Frameworks. *J. Am. Chem. Soc.* **2012**, *134*, 406–417.
191. Roy, I.; Stoddart, J. F. Cyclodextrin Metal–Organic Frameworks and Their Applications. *Acc. Chem. Res.* **2021**, *54*, 1440–1453.
192. Chen, L. X.; Liu, M.; Zhang, Y. Q.; Zhu, Q. J.; Liu, J. X.; Zhu, B. X.; Tao, Z. Outer Surface Interactions to Drive Cucurbit[8]uril-Based Supramolecular Frameworks: Possible Application in Gold Recovery. *Chem. Commun.* **2019**, *55*, 14271–14274.
193. Lin, R.-L.; Dong, Y.-P.; Tang, M.; Liu, Z.; Tao, Z.; Liu, J.-X. Selective Recovery and Detection of Gold with Cucurbit[*n*]urils (n = 5–7). *Inorg. Chem.* **2020**, *59*, 3850–3855.
194. Wu, H.; Jones, L. O.; Wang, Y.; Shen, D.; Liu, Z.; Zhang, L.; Cai, K.; Jiao, Y.; Stern, C. L.; Schatz, G. C.; Stoddart, J. F. High-Efficiency Gold Recovery Using Cucurbit[6]uril. *ACS Appl. Mater. Interfaces* **2020**, *12*, 38768–38777.
195. Dong, C. C.; Xiang, J. F.; Xu, L. J.; Gong, H. Y. MCl_4^{n-} ($AuCl_4^-$, $PtCl_4^{2-}$, or $PdCl_4^{2-}$) Anion Extraction from Na_nMCl_4 in Water Using a Tetraimidazolium Macrocyclic Receptor. *Tetrahedron Lett.* **2018**, *59*, 264–267.
196. Liu, W.; Oliver, A. G.; Smith, B. D. Macrocyclic Receptor for Precious Gold, Platinum, or Palladium Coordination Complexes. *J. Am. Chem. Soc.* **2018**, *140*, 6810–6813.
197. Wang, L.-L.; Tu, Y.-K.; Yao, H.; Jiang, W. 2,3-Dibutoxynaphthalene-Based Tetralactam Macrocycles for Recognizing Precious Metal Chloride Complexes. *Beilstein J. Org. Chem.* **2019**, *15*, 1460–1467.
198. Shaffer, C. C.; Liu, W.; Oliver, A. G.; Smith, B. D. Supramolecular Paradigm for Capture and Co-Precipitation of Gold(III) Coordination Complexes. *Chem. Eur. J.* **2021**, *27*, 751–757.
199. Grommet, A. B.; Feller, M.; Klajn, R. Chemical Reactivity Under Nanoconfinement. *Nat. Nanotech.* **2020**, *15*, 256–271.
200. Merlau, M. L.; Mejia, M. D. P.; Nguyen, S. T.; Hupp, J. T. Artificial Enzymes Formed through Directed Assembly of Molecular Square Encapsulated Epoxidation Catalysts. *Angew. Chem. Int. Ed.* **2001**, *40*, 4239–4242.
201. Breslow, R.; Overman, L. E. An "Artificial Enzyme" Combining a Metal Catalytic Group and a Hydrophobic Binding Cavity. *J. Am. Chem. Soc.* **1970**, *92*, 1075–1077.
202. Breslow, R.; Zhang, B. Cleavage of Phosphate Esters by a Cyclodextrin Dimer Catalyst That Binds the Substrates together with La^{3+} and Hydrogen Peroxide. *J. Am. Chem. Soc.* **1994**, *116*, 7893–7894.
203. Breslow, R. Biomimetic Chemistry and Artificial Enzymes: Catalysis by Design. *Acc. Chem. Res.* **1995**, *28*, 146–153.
204. Breslow, R.; Zhang, X.; Xu, R.; Maletic, M.; Merger, R. Selective Catalytic Oxidation of Substrates that Bind to Metalloporphyrin Enzyme Mimics Carrying Two or Four Cyclodextrin Groups and Related Metallosalens. *J. Am. Chem. Soc.* **1996**, *118*, 11678–11679.
205. Zhang, B.; Breslow, R. Ester Hydrolysis by a Catalytic Cyclodextrin Dimer Enzyme Mimic with a Metallobipyridyl Linking Group. *J. Am. Chem. Soc.* **1997**, *119*, 1676–1681.
206. Breslow, R.; Dong, S. D. Biomimetic Reactions Catalyzed by Cyclodextrins and Their Derivatives. *Chem. Rev.* **1998**, *98*, 1997–2011.
207. Baugh, S. D. P.; Yang, Z.; Leung, D. K.; Wilson, D. M.; Breslow, R. Cyclodextrin Dimers as Cleavable Carriers of Photodynamic Sensitizers. *J. Am. Chem. Soc.* **2001**, *123*, 12488–12494.
208. Breslow, R. Artificial Enzymes. *Science* **2006**, *218*, 532–537.

DOI: 10.31635/ccschem.021.202101286
Corrected Citation: *CCS Chem.* **2022**, 4, 755–784
Previous Citation: *CCS Chem.* **2021**, 3, 3436–3465
Link to VoR: https://doi.org/10.31635/ccschem.021.202101286

209. Koblenz, T. S.; Wassenaar, J.; Reek, J. N. H. Reactivity within a Confined Self-Assembled Nanospace. *Chem. Soc. Rev.* **2008**, *37*, 247–262.
210. Raynal, M.; Ballester, P.; Vidal-Ferran, A.; Van Leeuwen, P. W. N. M. Supramolecular Catalysis. Part 2: Artificial Enzyme Mimics. *Chem. Soc. Rev.* **2014**, *43*, 1734–1787.
211. Brown, C. J.; Toste, F. D.; Bergman, R. G.; Raymond, K. N. Supramolecular Catalysis in Metal–Ligand Cluster Hosts. *Chem. Rev.* **2015**, *115*, 3012–3035.
212. Roland, S.; Suarez, J. M.; Sollogoub, M. Confinement of Metal–*N*-Heterocyclic Carbene Complexes to Control Reactivity in Catalytic Reactions. *Chem. Eur. J.* **2018**, *24*, 12464–12473.
213. Jongkind, L. J.; Caumes, X.; Hartendorp, A. P. T.; Reek, J. N. H. Ligand Template Strategies for Catalyst Encapsulation. *Acc. Chem. Res.* **2018**, *51*, 2115–2128.
214. Tan, C.; Chu, D.; Tang, X.; Liu, Y.; Xuan, W.; Cui, Y. Supramolecular Coordination Cages for Asymmetric Catalysis. *Chem. Eur. J.* **2019**, *25*, 662–672.
215. Fang, Y.; Powell, J. A.; Li, E.; Wang, Q.; Perry, Z.; Kirchon, A.; Yang, X.; Xiao, Z.; Zhu, C.; Zhang, L.; Huang, F.; Zhou, H. C. Catalytic Reactions within the Cavity of Coordination Cages. *Chem. Soc. Rev.* **2019**, *48*, 4707–4730.
216. Morimoto, M.; Bierschenk, S. M.; Xia, K. T.; Bergman, R. G.; Raymond, K. N.; Toste, F. D. Advances in Supramolecular Host-Mediated Reactivity. *Nat. Catal.* **2020**, *3*, 969–984.
217. Wang, K.; Jordan, J. H.; Hu, X. Y.; Wang, L. Supramolecular Strategies for Controlling Reactivity within Confined Nanospaces. *Angew. Chem. Int. Ed.* **2020**, *59*, 13712–13721.
218. Mitschke, B.; Turberg, M.; List, B. Confinement as a Unifying Element in Selective Catalysis. *Chem* **2020**, *6*, 2515–2532.
219. Trouvé, J.; Gramage-Doria, R. Beyond Hydrogen Bonding: Recent Trends of Outer Sphere Interactions in Transition Metal Catalysis. *Chem. Soc. Rev.* **2021**, *50*, 3565–3584.
220. Zhang, P.; Meijide Suárez, J.; Driant, T.; Derat, E.; Zhang, Y.; Ménand, M.; Roland, S.; Sollogoub, M. Cyclodextrin Cavity-Induced Mechanistic Switch in Copper-Catalyzed Hydroboration. *Angew. Chem. Int. Ed.* **2017**, *129*, 10961–10965.
221. Xu, G.; Leloux, S.; Zhang, P.; Meijide Suárez, J.; Zhang, Y.; Derat, E.; Ménand, M.; Bistri-Aslanoff, O.; Roland, S.; Leyssens, T.; Riant, O.; Sollogoub, M. Capturing the Monomeric (L)CuH in NHC-Capped Cyclodextrin: Cavity-Controlled Chemoselective Hydrosilylation of α,β-Unsaturated Ketones. *Angew. Chem. Int. Ed.* **2020**, *59*, 7591–7597.
222. Hong, C. M.; Bergman, R. G.; Raymond, K. N.; Toste, F. D. Self-Assembled Tetrahedral Hosts as Supramolecular Catalysts. *Acc. Chem. Res.* **2018**, *51*, 2447–2455.
223. Bender, T. A.; Bergman, R. G.; Raymond, K. N.; Toste, F. D. A Supramolecular Strategy for Selective Catalytic Hydrogenation Independent of Remote Chain Length. *J. Am. Chem. Soc.* **2019**, *141*, 11806–11810.
224. Bender, T. A.; Morimoto, M.; Bergman, R. G.; Raymond, K. N.; Toste, F. D. Supramolecular Host-Selective Activation of Iodoarenes by Encapsulated Organometallics. *J. Am. Chem. Soc.* **2019**, *141*, 1701–1706.
225. García-Simón, C.; Gramage-Doria, R.; Raoufmoghaddam, S.; Parella, T.; Costas, M.; Ribas, X.; Reek, J. N. H. Enantioselective Hydroformylation by a Rh-Catalyst Entrapped in a Supramolecular Metallocage. *J. Am. Chem. Soc.* **2015**, *137*, 2680–2687.
226. Slagt, V. F.; Reek, J. N. H.; Kamer, P. C. J.; Van Leeuwen, P. W. N. M. Assembly of Encapsulated Transition Metal Catalysts. *Angew. Chem. Int. Ed.* **2001**, *40*, 4271–4274.
227. Bocokić, V.; Kalkan, A.; Lutz, M.; Spek, A. L.; Gryko, D. T.; Reek, J. N. H. Capsule-Controlled Selectivity of a Rhodium Hydroformylation Catalyst. *Nat. Commun.* **2013**, *4*, 1–9.
228. Nurttila, S. S.; Linnebank, P. R.; Krachko, T.; Reek, J. N. H. Supramolecular Approaches to Control Activity and Selectivity in Hydroformylation Catalysis. *ACS Catal.* **2018**, *8*, 3469–3488.
229. Slagt, V. F.; Kamer, P. C. J.; Van Leeuwen, P. W. N. M.; Reek, J. N. H. Encapsulation of Transition Metal Catalysts by Ligand-Template Directed Assembly. *J. Am. Chem. Soc.* **2004**, *126*, 1526–1536.
230. Kuil, M.; Soltner, T.; Van Leeuwen, P. W. N. M.; Reek, J. N. H. High-Precision Catalysts: Regioselective Hydroformylation of Internal Alkenes by Encapsulated Rhodium Complexes. *J. Am. Chem. Soc.* **2006**, *128*, 11344–11345.
231. Rayder, T. M.; Bensalah, A. T.; Li, B.; Byers, J. A.; Tsung, C. Engineering Second Sphere Interactions in a Host–Guest Multicomponent Catalyst System for the Hydrogenation of Carbon Dioxide to Methanol. *J. Am. Chem. Soc.* **2021**, *143*, 1630–1640.
232. Cardin, C. J.; Kelly, J. M.; Quinn, S. J. Photochemically Active DNA-Intercalating Ruthenium and Related Complexes—Insights by Combining Crystallography and Transient Spectroscopy. *Chem. Sci.* **2017**, *8*, 4705–4723.
233. Hall, J. P.; O'Sullivan, K.; Naseer, A.; Smith, J. A.; Kelly, J. M.; Cardin C. J. Structure Determination of an Intercalating Ruthenium Dipyridophenazine Complex which Kinks DNA by Semiintercalation of a Tetraazaphenanthrene Ligand. *Proc. Natl. Acad. Sci. U. S. A.* **2011**, *108*, 17610–17614.
234. Song, H.; Kaiser, J. K.; Barton, J. K. Crystal Structure of Δ-$[Ru(bpy)_2dppz]^{2+}$ Bound to Mismatched DNA Reveals Side-by-side Metalloinsertion and Intercalation. *Nat. Chem.* **2012**, *4*, 615–620.
235. Niyazi, H.; Hall, J. P.; O'Sullivan, K.; Winter, G.; Sorensen, T.; Kelly, J. M.; Cardin, C. J. Crystal Structures of Λ-$[Ru(phen)_2(dppz)]^{2+}$ with Oligonucleotides Containing TA/TA and AT/AT Steps Show Two Intercalation Modes. *Nat. Chem.* **2012**, *4*, 621–628.
236. Hall, J. P.; Poynton, F. E.; Keane, P. M.; Gurung, S. P.; Brazier, J. A.; Cardin, D. J.; Winter, G.; Gunnlaugsson, T.; Sazanovich, I. V.; Towrie, M.; Cardin, C. J.; Kelly, J. M.; Quinn, S. J. Monitoring One-Electron Photo-Oxidation of Guanine in DNA Crystals Using Ultrafast Infrared Spectroscopy. *Nat. Chem.* **2015**, *7*, 961–967.
237. Vukotic, V. N.; Harris, K. J.; Zhu, K.; Schurko, R. W.; Loeb, S. J. Metal–Organic Frameworks with Dynamic Interlocked Components. *Nat. Chem.* **2012**, *4*, 456–460.
238. Zhu, K.; Vukotic, V. N.; Okeefe, C. A.; Schurko, R. W.; Loeb, S. J. Metal–Organic Frameworks with Mechanically Interlocked Pillars: Controlling Ring Dynamics in the Solid-State via a Reversible Phase Change. *J. Am. Chem. Soc.* **2014**, *136*, 7403–7409.

DOI: 10.31635/ccschem.021.202101286
Corrected Citation: *CCS Chem.* **2022**, 4, 755–784
Previous Citation: *CCS Chem.* **2021**, 3, 3436–3465
Link to VoR: https://doi.org/10.31635/ccschem.021.202101286

239. Zhu, K.; O'Keefe, C. A.; Vukotic, V. N.; Schurko, R. W.; Loeb, S. J. A Molecular Shuttle that Operates inside a Metal–Organic Framework. *Nat. Chem.* **2015**, *7*, 514–519.
240. Wilson, B. H.; Loeb, S. J. Integrating the Mechanical Bond into Metal–Organic Frameworks. *Chem* **2020**, *6*, 1604–1612.
241. Wilson, B. H.; Vojvodin, C. S.; Gholami, G.; Abdulla, L. M.; O'Keefe, C. A.; Schurko, R. W.; Loeb, S. J. Precise Spatial Arrangement and Interaction between Two Different Mobile Components in a Metal-Organic Framework. *Chem* **2021**, *7*, 202–211.

DOI: 10.31635/ccschem.021.202101286
Corrected Citation: *CCS Chem.* **2022**, 4, 755–784
Previous Citation: *CCS Chem.* **2021**, 3, 3436–3465
Link to VoR: https://doi.org/10.31635/ccschem.021.202101286